LA-UR-93-3448

LOS ALAMOS NATIONAL LABORATORY

ACCELERATOR PRODUCTION OF TRITIUM PROJECT

B&R GB0508302

APT RADIONUCLIDE PRODUCTION EXPERIMENT

TECHNICAL REPORT

September 1993

Submitted to

US Department of Energy
Office of Weapons Complex Reconfiguration, DP 40

LOS ALAMOS NATIONAL LABORATORY
Acclerator Production of Tritium (APT) Project Office
RADIONUCLIDE PRODUCTION TECHNICAL REPORT
Review and Approval Form

Chapter No.	Prepared by:	Date & Signature	Reviewed by:	Date & Signature
1	J. Ullmann	9/30/93	F. Venneri	9-29-93
2	↓	↓	↓	↓
3				
4				
5				
6				
7				
8				
9				
10				
11				
12				
13				
14				
15				
16				
Appendix	J. Ullmann	9/30/93	F. VENNERI	9-29-93

Approved: P. Lisowski — Task Leader Name — Date & Signature

Approved: J. Ireland — APT Project Manager — 9/30/93 — Date & Signature

Participants

Group P-17

J.L. Ullmann
J. King
P.W. Lisowski
R.O. Nelson
S.A. Wender
D. Jagnow
A. Gavron
J. Koster
D. Mayo
L. Waters
C. Zoeller
R. Laird

Group INC-13

G. Butler
R. Gritzo
M.A. Yates
M. Fowler
J. Wilhelmy

Group T-2

W. Wilson

1. Introduction

Tritium (^3H, a heavy isotope of hydrogen) is produced by low energy neutron-induced reactions on various elements. One such reaction is $n+^3He \rightarrow ^3H+^1H$ in which ^3He is transmuted to tritium. Another reaction, which has been used in reactor production of tritium, is the $n+^6Li \rightarrow ^3H+^4He$ reaction. Accelerator Production of Tritium relies on a high-energy proton beam to produce these neutrons using the spallation reaction, in which high-energy protons reacting with a heavy nucleus produce a shower of low-energy neutrons and a lower-mass residual nucleus. It is important to quantify the residual radionuclides produced in the spallation target for two reasons. From an engineering point of view, one must understand short-lived isotopes that may contribute to decay heat. From a safety viewpoint, one must understand what nuclei and decay gammas are produced in order to design adequate shielding, to estimate ultimate waste disposal problems, and to predict possible effects due to accidental dispersion during operation.

Because stopping-length targets (i.e. targets in which the initial protons will lose all their energy prior to coming to a stop) will be used for neutron production, radionuclide production over a wide energy range must be considered. The calculation of radionuclide production in a thick target involves two different processes. First, the transport of the incident particles and their reaction products, including neutrons, must be considered in detail. Second, the probability for production of a given radionuclide in a reaction must be calculated.

Although numerous measurements of thin-target radionuclide production have been made, there have been only a few measurements of stopping-length systems [1,2]. The most complete study, described in [1], showed results for Pb and U targets, but was not completely analyzed or published.

The design of targets for neutron production using spallation involves elaborate calculations with Monte-Carlo transport and particle production codes. These codes follow every particle produced until it either slows down to the point of stopping, or vanishes due to the interaction with an atomic nucleus. This tracking takes place through elaborate geometric structures involving many different materials. The probability that a particle will interact at any point in a material is determined by its "cross-section". The cross-section is a characteristic property of each nucleus, and varies with the energy and the species (i.e., proton, neutron,...) of the impinging particle. When a particle interacts, other particles may be produced or the incoming particle may be scattered to a new direction. The probability for a particle to interact and produce one or more particles in a given direction and with a given energy is termed a "double-differential" cross-section, and denoted $d^2\sigma/dEd\Omega$. These cross-sections need to be known for all the elements and for all particles and energies that could be produced in a spallation target in order to be able to accurately track the initial particle and the subsequent generations of particles produced in a target. For neutrons up to

energies of 20 MeV, numerous measurements of $d^2\sigma/dEd\Omega$ have been made. They have been incorporated in vast libraries used by the MCNP (Monte-Carlo Neutron and Photon) code for tracking neutrons [3].

Very few measurements of the double-differential cross section have been made for neutrons at higher energies, or for all other particles. The current status of experimental data is discussed in several reviews [4,5,6,7]. Where cross sections are not available, the calculations use physics models. One such model, the Intra-Nuclear Cascade (INC) model, uses a simple approach that assumes that a nucleon colliding with a nucleus may be described in terms of scattering the incoming nucleon off the individual nuclear constituents. This model describes the overall features of high-energy scattering, such as the high energy of the forward-going particles, and qualitatively reproduces $d^2\sigma/dEd\Omega$ at energies above about 200 MeV and angles greater than 10 degrees [4]. In the INC calculation, energy is deposited in the struck nucleus. This energy is then dissipated by the evaporation of low energy particles. The evaporation model provides a reasonable description of cross-sections, but often does not get the correct ratio between the different kinds of emitted particles.

Consequently, the transport calculations performed using MCNP and the Los Alamos High Energy Transport code (LAHET) [8] are not completely accurate. It is generally believed that when they are used to determine average numbers, such as the total number of emitted neutrons or the total radioisotope production, one can expect errors of the order of ~20%. However, more specific details, such as the production of a specific radioisotope, may be in error by a much larger amount. It is therefore necessary to experimentally benchmark these calculations in a configuration resembling that to be used in the final construction. We have performed an experiment to measure the production of radioisotopes in stoppping-length W and Pb targets irradiated by a 800 MeV proton beam, and are comparing the results to values obtained from calculations using LAHET and MCNP. The experiment was designed to pay particular attention to the short half-life radionuclides, which have not been previously measured. In the following, we present details of the experiment, explain how we analyze the data and obtain the results, how we perform the calculations, and finally, how the experimental data agree with the calculations.

2. Experimental Method

The experiment was done using the "Target 2" external proton beam at the WNR (Weapons Neutron Research) facility at LAMPF. This area is fed by the H^- beam from the LAMPF linear accelerator at energies up to 800 MeV. A diagram of the WNR facility is shown in Figure 1.

Thick tungsten and lead targets were irradiated with 800 MeV protons. Thin foils were inserted at various locations to sample the radiation environment inside the target . The foils

were then removed and counted using high-resolution high-purity germanium gamma-ray detectors. The radioisotopes produced were then identified through their characteristic gamma-ray energy spectra.

The tungsten target, shown in Fig. 2, was 45.7 cm long and 20.3 cm square. A lead shield was placed on the front of the target to protect personnel from the high-activation region where the beam enters the target. Foils could be inserted at 5-cm intervals from the front of the target. Fig. 3a. shows a diagram of the Pb target. Foils were held in a lexan polycarbonate holder, similar to the Pb foil holder shown in Fig. 3b. The foils inserted on the beam axis were to measure interactions due primarily to the incident beam; the off-axis foils sampled interactions due to scattered and secondary particles (primarily neutrons.) The foils were 0.191 cm (0.750 in) diameter disks, with nominal thickness of either 0.051 cm (0.020 in) or 0.102 cm (0.040 in.)

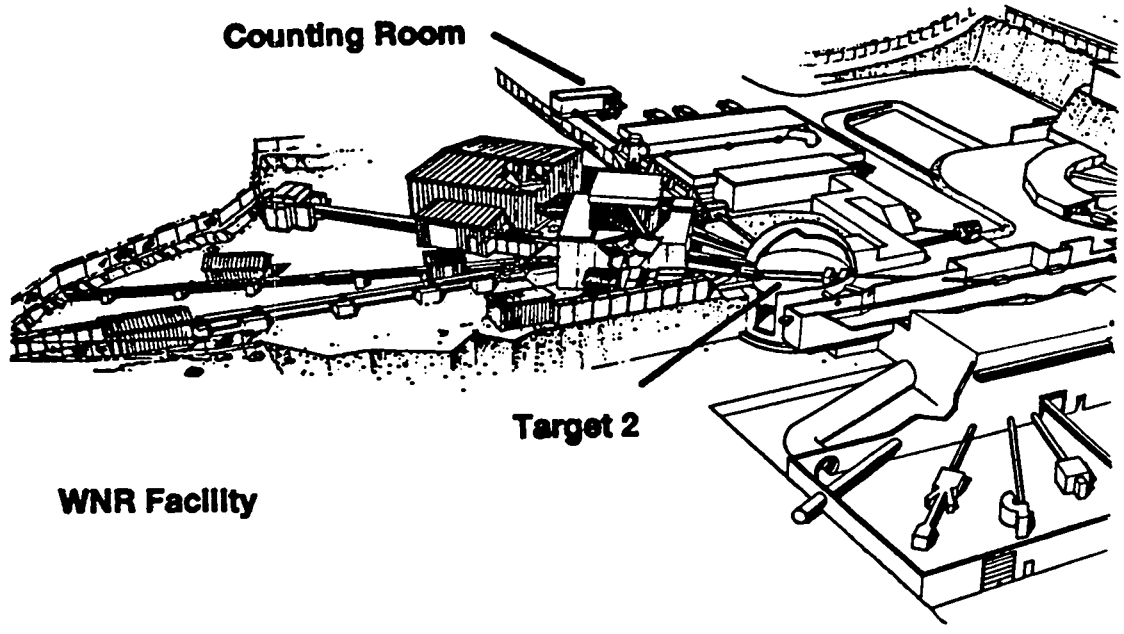

Fig. 1. The WNR Facility at LAMPF. Beam is delivered from the LINAC off the page to the right. Target 2 and the counting room for this experiment are indicated.

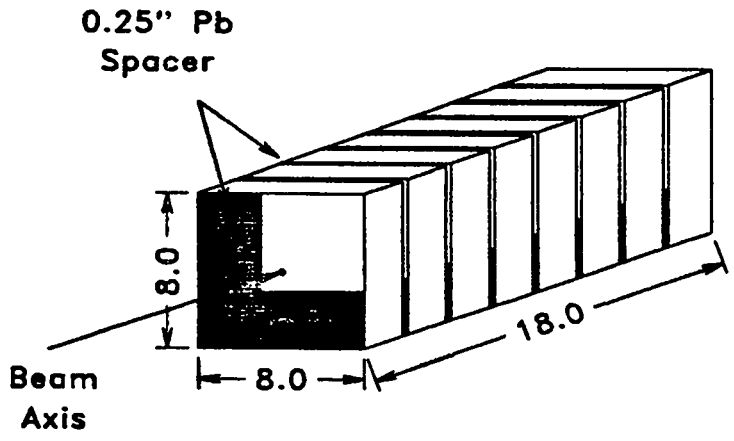

Fig 2. Drawing of the Tungsten target. Dimensions in inches.

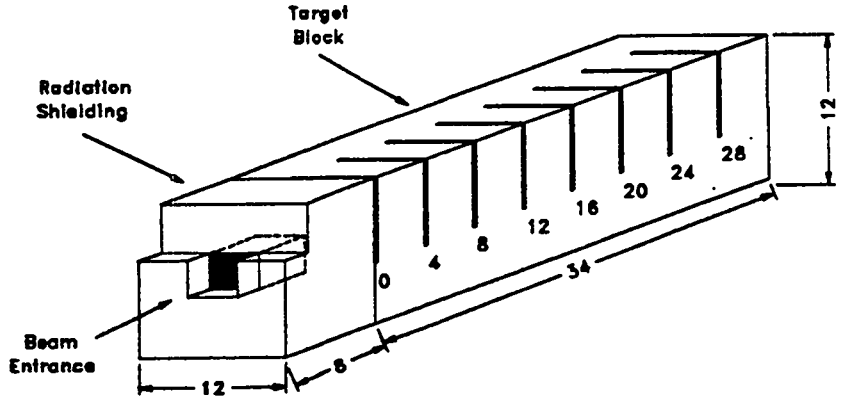

Fig 3a. Lead target. Dimensions are in inches.

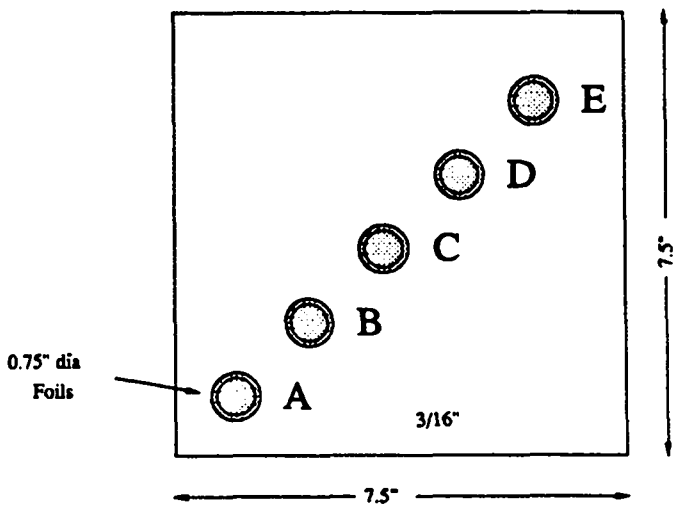

Fig. 3b. Lead target holder.

Irradiation times varied from a few seconds up to 8 hours, to study short-lived and long-lived isotopes respectively. This experiment represents the first study of short-lived thick-target W spallation products. Fourteen short irradiations, 1 one-hour, and 1 eight-hour tungsten irradiation were made. The W irradiations are summarized in Table 1. The proton beam fluence was determined by activation of thin aluminum foils. These foils were 0.00686 g/cm^2 for the 8 hr run, and 0.217 g/cm^2 for the shorter runs. Gamma rays from the decay of ^{24}Na produced in the ^{27}Al(p,3pn)^{24}Na were counted, and the absolute number of protons calculated using a value for the cross section of 10.94 ± 0.24 mb/sr [9]. Table 2 summarizes the Pb irradiations, but only shows an estimated proton fluence based on the average number of protons per beam micropulse, 3 x 10^8. The Al activation for the Pb runs has not yet been analyzed.

Table 1. Tungsten Irradiation Times

Run No.	Beam Pulses	Time (Sec)	Total number of protons
189	2,055	7	$8.33 \pm 0.65 \times 10^{11}$
191	3,000	10	$1.10 \pm 0.06 \times 10^{12}$
193	6,000	98	$2.53 \pm 0.09 \times 10^{12}$
195	20,000		
197	3,000	3	$9.17 \pm 0.57 \times 10^{11}$
199	5,000	6	$1.65 \pm 0.09 \times 10^{12}$
201	10,000	12	$3.01 \pm 0.10 \times 10^{12}$
206	20,000	31	$8.33 \pm 0.65 \times 10^{11}$
208	40,000	63	
210	80,000	125	$2.25 \pm 0.02 \times 10^{13}$
212	100,000	156	$2.18 \pm 0.05 \times 10^{13}$
214	1,150,081	3907	$3.31 \pm 0.01 \times 10^{14}$
214	4,309,096	21945	$2.58 \pm 0.04 \times 10^{15}$

Table 2. Lead Irradiation Times

Run No.	Beam Pulses	Time (Sec)	Estimated Total Protons
134	2,000	3	6.0×10^{11}
137	2,000	3	6.0×10^{11}
151	2,000	4	6.0×10^{11}
153	5,000	9	1.5×10^{12}
156	10,000	19	3.0×10^{12}
158	20,000	36	6.0×10^{12}
160	40,000	71	1.2×10^{13}
162	80,000	146	2.4×10^{13}
164	200,000	367	6.0×10^{13}
168	1,000,000	1352	3.0×10^{14}
182	5,453,113	4265	1.6×10^{15}

A germanium-detector counting system was set up at the WNR so that the short-irradiation foils could be counted immediately for information on short-lived radioisotopes. A procedure was developed so that target foils could be removed from the target and placed on the counters in about five minutes. Five Ge detector systems were set up in a CAMAC-based data acquisition system using the acquisition program XSYS. A diagram of the associated electronics is shown in Fig. 4. The electronics was designed to gate the proton beam on for a preset number of pulses, wait a predetermined interval, and then gate the ADC's on and off for a number of counting intervals. Typically, the waiting interval between beam off and the first count was set to be 5.00 minutes, and fifteen counts of 3.00 minutes each were taken. From this series of counts, the half-life of the radionuclides could be determined. The electronics was designed to allow individual counting intervals for each detector, but this feautre was not used. The system also counted the number of beam pulses, measured the exact start and stop time of each count, and determined the deadtime of the system.

The foils from the one-hour runs were first counted at the WNR, and then transported to the automated counting facility of the Isotope and Nuclear Chemistry (INC) Division. All of the foils from the eight-hour irradiations were counted at INC. These counts were made for up to 35 days after end of bombardment and were counted for longer periods of time, typically 50 to 100 minutes each.

The detectors were calibrated for energy and detector efficiency using a commercial standard source traceable to NIST [10]. However, the thick foils used in the irradiation transmitted

only about 10% of the lower energy gamma rays, making a precise determination of the product of efficiency and transmission very important. This was calculated using the computer code EFFIC [11], which was verified against the standard source. A typical efficiency curve for several foil thicknesses on WNR detector five is shown in Figure 6.

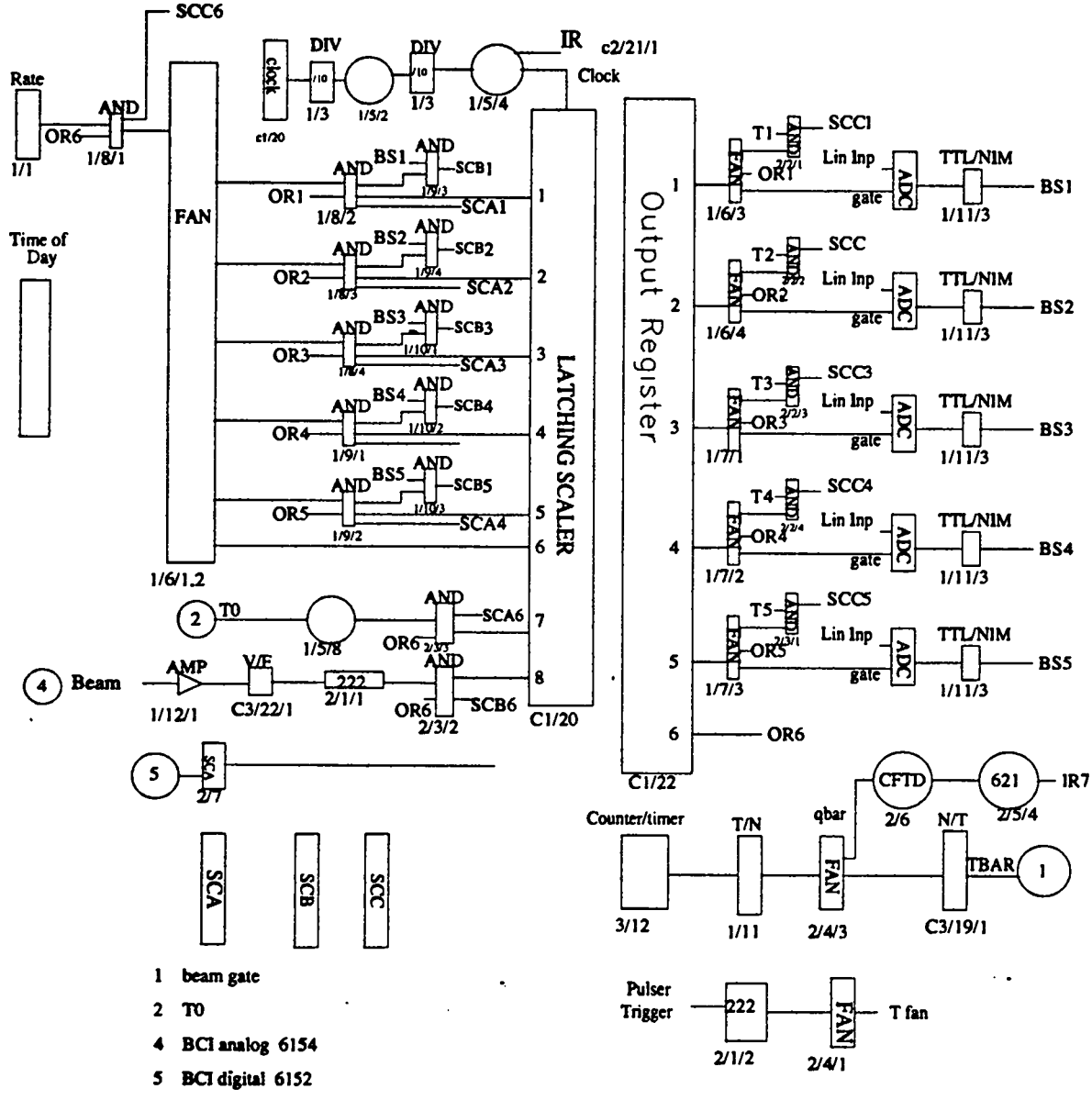

Fig. 4. Electronics diagram for APT Experiment.

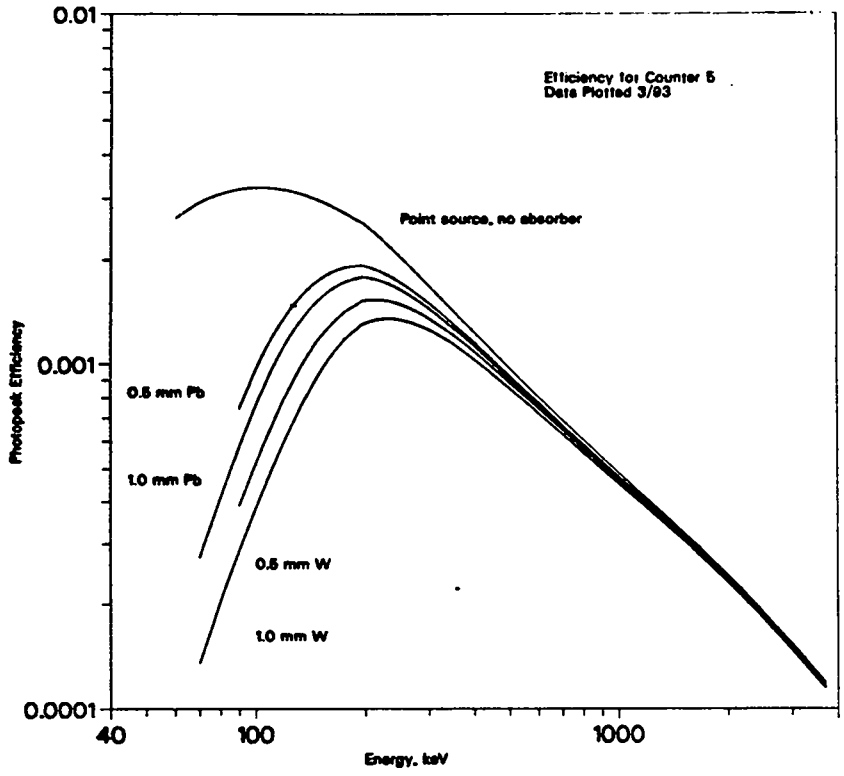

Fig. 6. Calculated efficiency curve for WNR Detector 5. The efficiency for various thickness foils is shown.

Approximately 2500 spectra were obtained from the short half-life runs, each containing approximately 100 analyzable peaks. About five-hundred spectra were measured at longer times, each containing 200 to 300 peaks. Gamma peak areas were determined by the automated peak-fitting code GAMANAL [12]. This code internally optimizes the energy calibration, peak shape parameters and background using known peaks in the measured spectrum. The energy determination was accurate typically to less than 1 keV. Radionuclide identification was suggested by GAMANAL based on a gamma-ray library, and then checked against half-life. The internal gamma-ray library was updated to include candidate spallation-product nuclei using the tabulation of Spanier and Ekstrom [13], which was based on the ENDF compilation of March 8, 1989.

Sample gamma-ray spectra from the one hour W irradiation are shown in Fig. 7. The spectra are from a tungsten foil in position 4A, and are shown after several decay times. It is interesting to note several regions of the spectrum. The peak at about channel 600 (300 kev) has about the same strength at all times, indicating a very long half life. The peaks near channel 2000 (approx. 1000 keV) show more structure at long decay times, perhaps indicating parent-daughter buildup, while the peaks near channel 3500 (approx 1750 keV) die away at longer times, indicating decay.

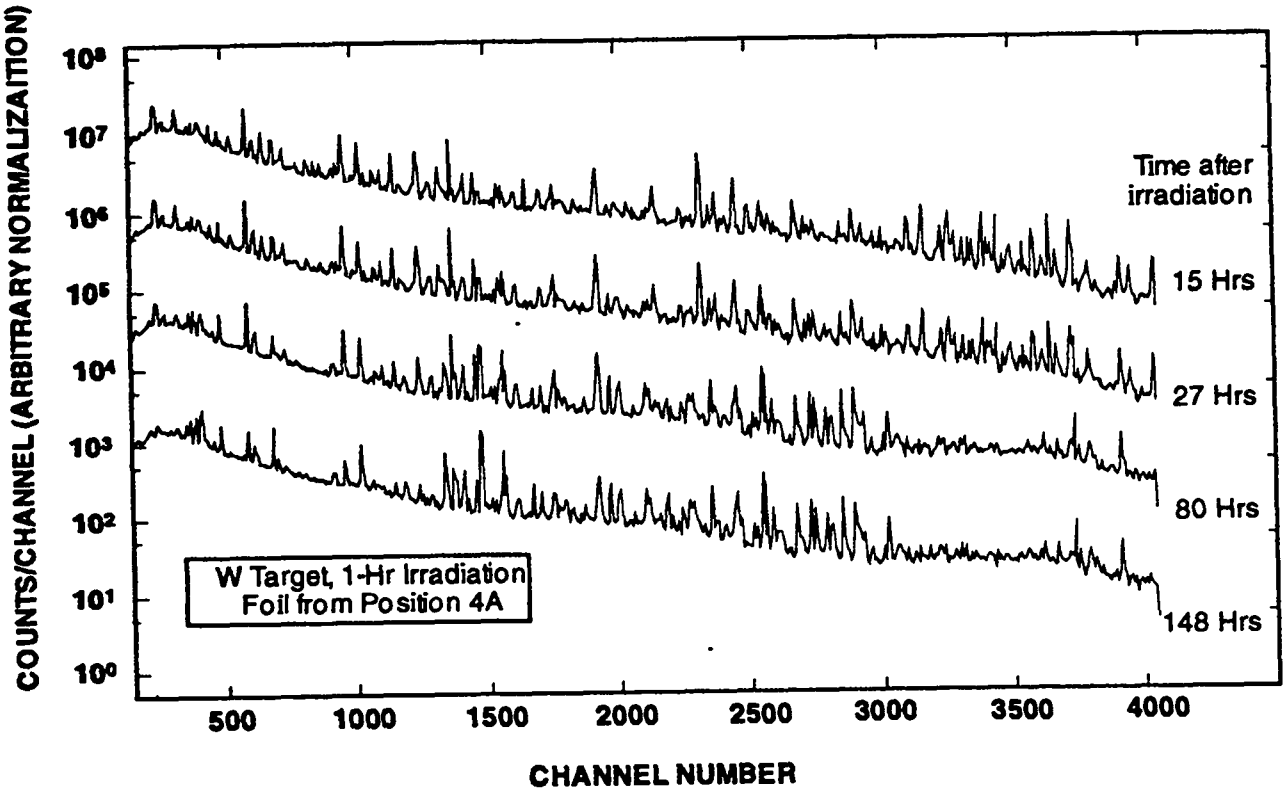

Fig. 7. Several W spectra at different decay times from foil 614, taken using the INC counting facility. The approximate energy calibration is 0.5 keV/channel.

3. Model Calculations

Initially we consider scoping calculations in a simple geometry, a tungsten cylinder 40 cm long and 20 cm radius. These calculations demonstrate the properties of spallation with 800 MeV protons, and subsequent transport and interactions of the secondary particles. One measure of the distribution of particles is the energy deposited by them in individual volume elements. Figure 8 depicts the energy deposited per unit mass (MeV/g) due to the high-energy particles (primary beam and all secondaries, except neutrons below 20 MeV) as calculated by LAHET.

We note that most of the energy deposition is concentrated in the first ~15 cm depth and ~5 cm radius, with extended tails out to longer distances and larger radii. The energy deposition due to low-energy neutron induced reactions, calculated using MCNP, is presented in Fig. 9. These low energy neutrons ($E \leq 20$ MeV) have a long mean-free-path (average distance between interactions) and spread around over much larger volumes. They are the primary source of activation products far from the beam axis, and deep inside the cylinder. These neutrons are the basis for the APT and ATW projects, where their high fluxes are utilized for tritium production and waste transmutation.

Figure 10 depicts the mass distribution of spallation products 2 cm deep inside the cylinder, as a function of the radius. Close to the beam, the mass yield contains many low-mass products, which result from a large number of particles removed from the target nucleus. This implies that the nucleus was hit by a high-energy particle, which had the energy to remove a lot of mass. At larger radii, the mass distribution is much narrower, since the particles at these radii have much less energy, and consequently cannot remove as many particles from the target nucleus. Figure 11 shows the mass distribution as one goes deeper into the cylinder on the beam axis. Again, the mass distribution becomes narrower as the penetration goes deeper because the primary beam loses much of its energy, and the number of secondary, lower-energy particles increases. A different aspect of these processes is seen in Fig. 12. Here we compare mass yields from interactions of the primary beam to the total mass yield (from all particles) as a function of mass. Masses around that of tungsten evidently sample mainly secondary particles (their low energy causes emission of a very few particles), whereas masses around 160 sample the primary beam almost exclusively. Consequently, studying mass yields provides a large amount of information on the various physical processes. Deep inside the cylinder as well as at large radii, we are sampling spallation from secondary products and neutron activation. Near the beam center, we can study spallation due to both the primary beam and secondary particles using the mass distribution to discriminate between the different types of particles.

In the calculations used for comparison to the experimental data, the entire tungsten stack, lead shield, lexan holders, and foils were coded into LAHET and MCNP using their exact dimensions, with one exception: The tungsten foils themselves were assumed to have a 0.223 cm thickness and a 2.064 cm diameter, equal to the dimensions of the hole in the foil holder. This was done to increase the statistics of sampling by the simulation codes, in order to minimize statistical errors. It is not expected to cause any systematic error to the calculational results.

The full calculation ran 300,000 events of 800 MeV protons using LAHET. Neutrons from these events with energies below 20 MeV were written to a "NEUTP" file, and subsequently read and processed by MCNP. A listing of the input files for the LAHET and MCNP calculations is in Appendix A. The neutron flux produced in MCNP is used by CINDER'90 [14] to obtain a table of neutron activation products. The table of primary isotopes produced in spallation reactions was obtained from the LAHET "HISTP" file. These isotopes are then

transmuted using CINDER'90, which produces tables of activities of specific foils, broken down into the different isotopes producing the activity. This was done for different irradiation and different decay times, matching the irradiation and decay times in the experiment.

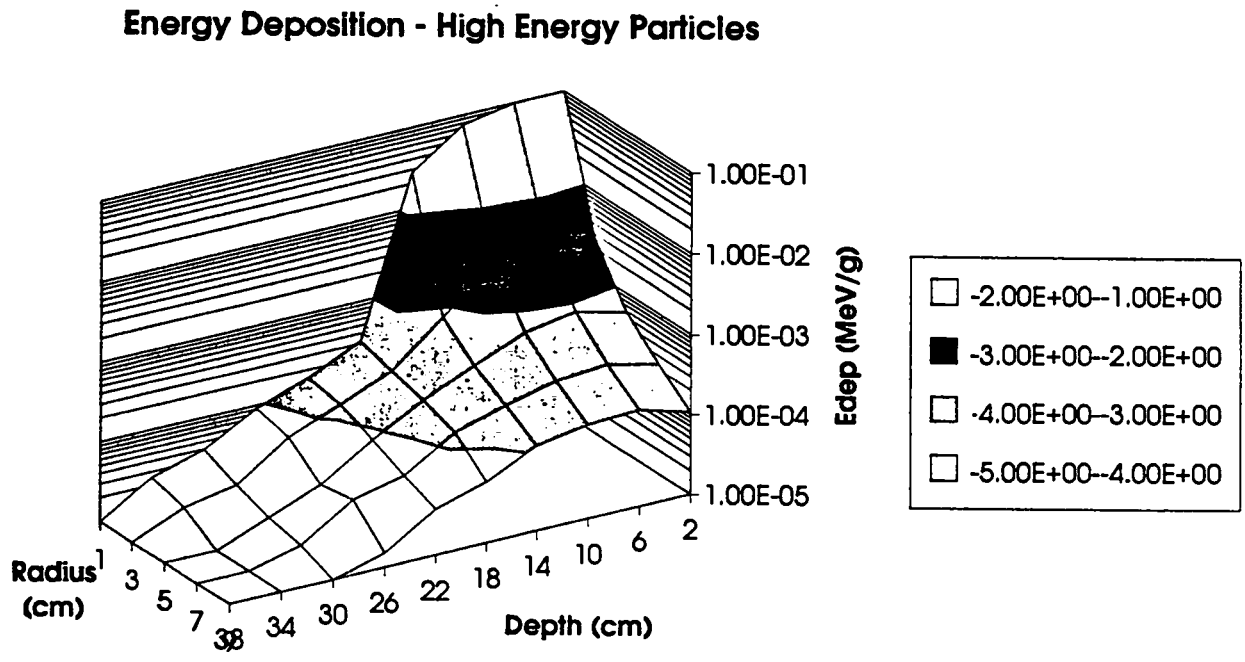

Fig. 8. Energy deposition as a function of radial position and depth in the cylinder. The legend indicates the power of 10 of the energy deposition.

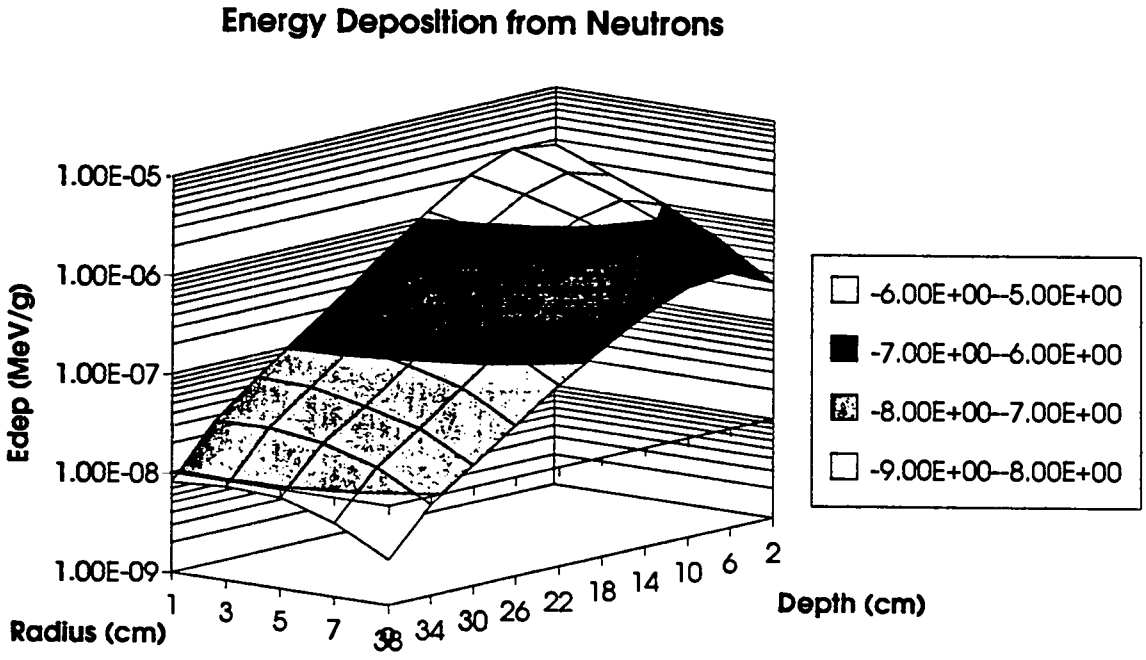

Fig. 9. Energy deposition from low- energy (<20 MeV) neutron-induced reactions, as a function of radial position and depth in the cylinder. The legend indicates the power of 10 of the energy deposition.

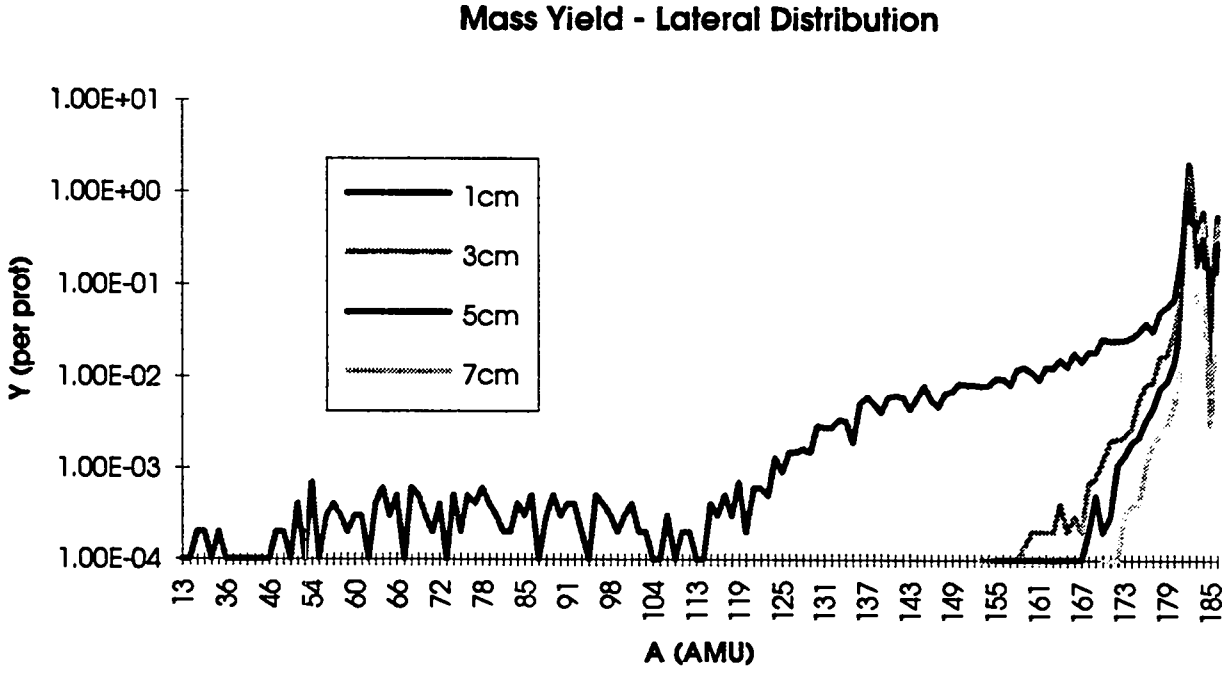

Fig. 10. Yield (as function of mass) of spallation products for different radii, at 2 cm depth in the cylinder. The top curve is for 2 cm radius, the bottom for 14 cm radius.

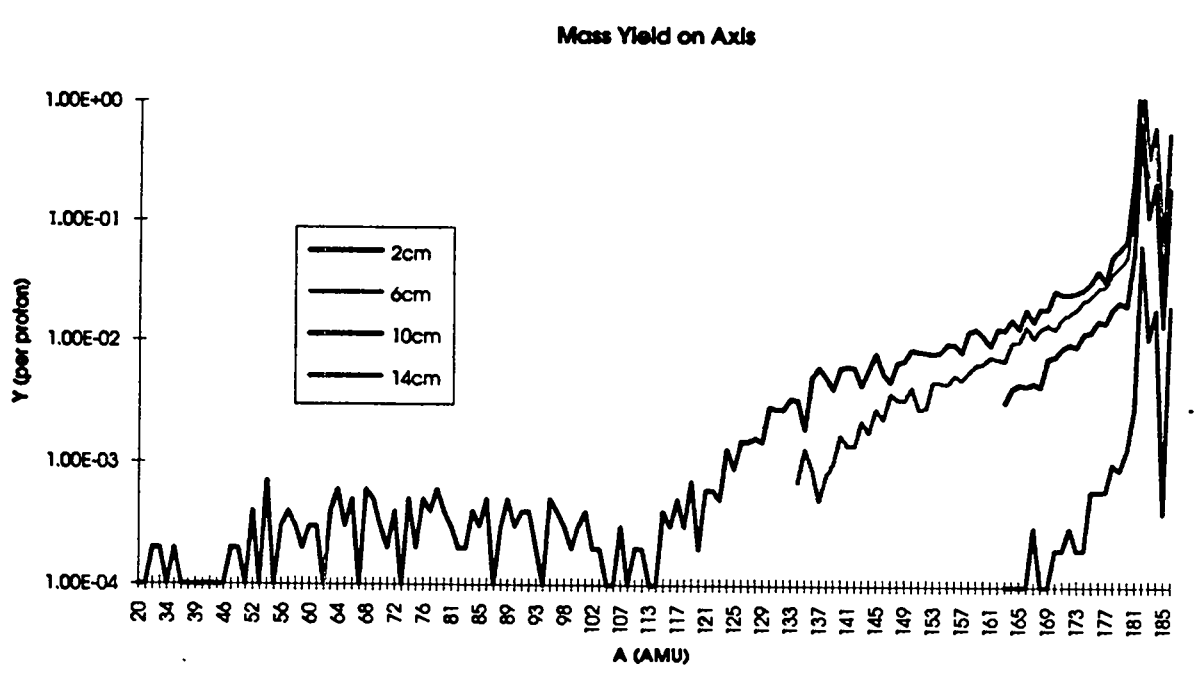

Fig. 11. Spallation mass yield on the beam axis, at different depths into the cylinder. The top curve is for 1 cm depth, the bottom for 7 cm depth.

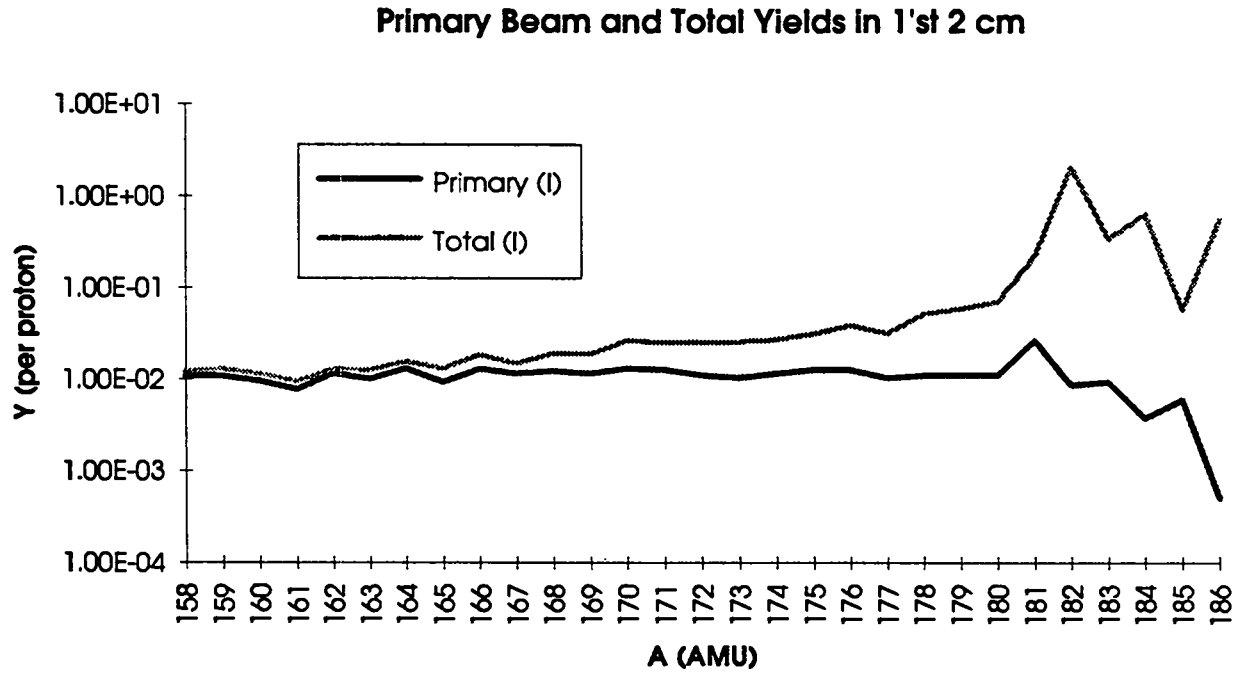

Fig. 12 On-axis mass yields from all reactions and from primary beam spallation only at 2 cm depth in cylinder.

4. Results

A very large set of data was collected, and the analysis, even though partially automated, is still very labor-intensive. For this reason, it was decided to begin the analysis with the W data, since W is an important element in the Los Alamos APT design and no thick-target spallation product data on W exists. A large amount of preliminary work was needed before spallation product yields could be determined. This work included determining an accurate energy and efficiency calibration for each detector, adapting the GAMANAL peak-fitting code to handle XSYS-generated data and correct for small but non-trivial nonlinearities in the WNR data-collection system, and updating the radionuclide library to include current data on medium-mass nuclei. After this preliminary work, the analysis effort was concentrated on foils in position 4A, on the beam axis 10 cm downstream from the front of the target.

The extracted yields, in nuclei/cm^3/proton, extrapolated from the first counting interval to the end of bombardment (EOB), are listed in Table 3a for the 6-second irradiation and in Table 3b for the 1-hour irradiation. Data from the 8-hour irradiation are still under analysis. It should be noted that the yields are averaged over the entire volume of the activated foil. For foils near the front of the target, where primary proton spallation dominates the production mechanism, the area of the beam may be less than the foil area.

The calculated yields [15] for the 6 second and 1 hour irradiations at position 4A are tabulated in Appendix B. The yields were calculated at end of bombardment and for the first, last, and middle counting interval.

Figure 13 shows the gamma-ray spectrum from the 1 hour irradiation, 140 hours after end of bombardment. Identified gamma rays are marked. Figure 14 is a summary of the ratio of measured to calculated yields, extrapolated to end of bombardment, for all identified nuclei. There are several caveats in interpreting this data. Many observed gamma lines have unresolved contributions from several different nuclei. In most cases we have not attempted to decompose these complex decays into their individual components. The results presented here depend primarily on gamma peaks with a unique decay scheme where possible, and on two-component gamma peaks which can be time-resolved into their individual decays. In addition, many of the nuclei calculated to be produced have decay schemes unfavorable for detection. These nuclei may have extremely short half lives, decay schemes that involve below-threshold gamma rays, or high-multiplicity peaks. Thus a comparison must be made only between observed and calculated yields. In most cases, an unobserved yield did not neccessarily imply that the nucleus was not produced.

Figure 15 is a histogram of the ratio of measured to calculated yields. In fifty-six percent of the nuclei, the calculated yield is within a factor of two of the meaurement. Finally, Fig. 16 shows the integral mass yield (sum of the spallation yields for all nuclei with a given mass) compared to the calculations [15].

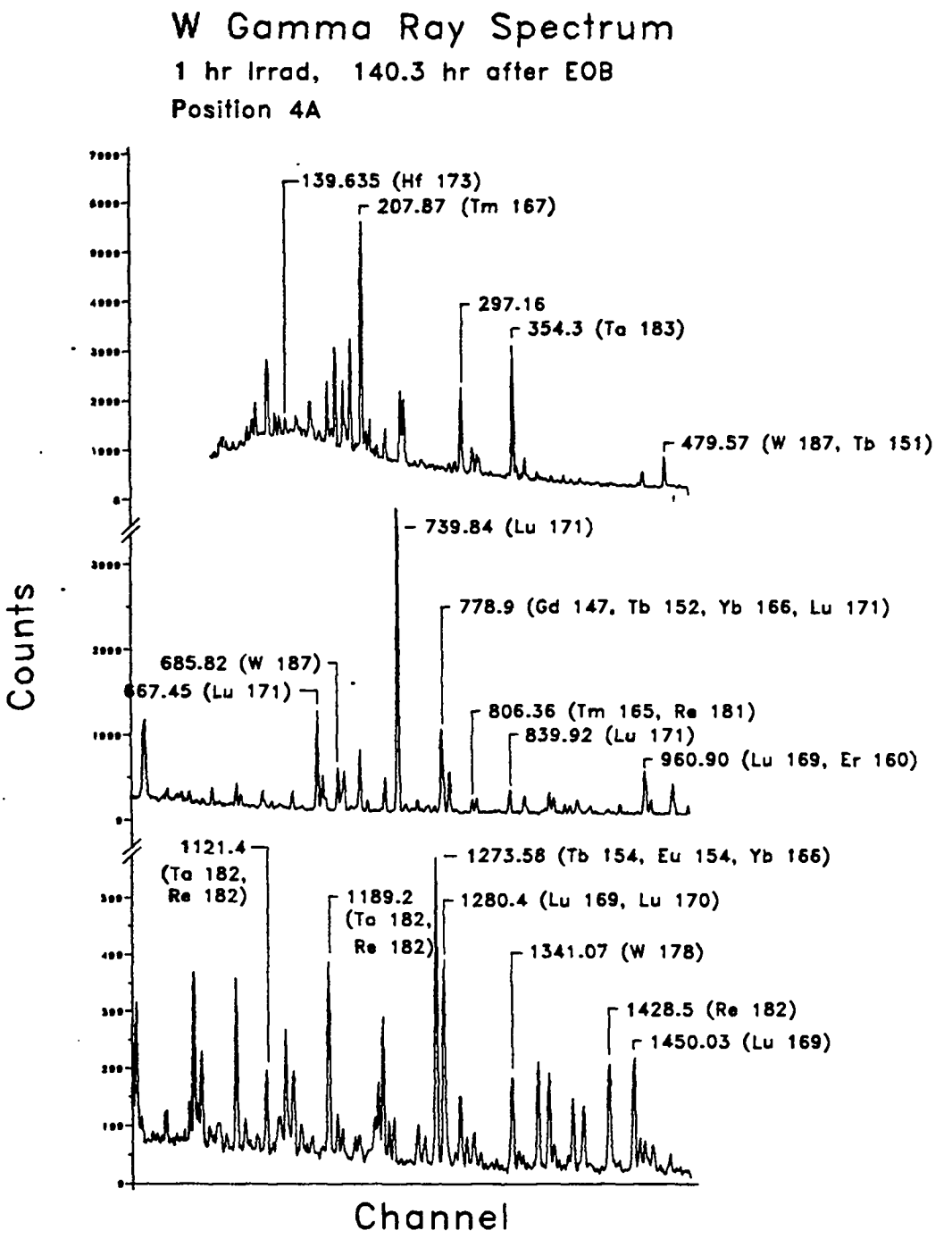

Fig 13. Tungsten gamma ray spectrum from on-axis position 4A (Foil 614) 140 hours after end of 1 hr bombardment.

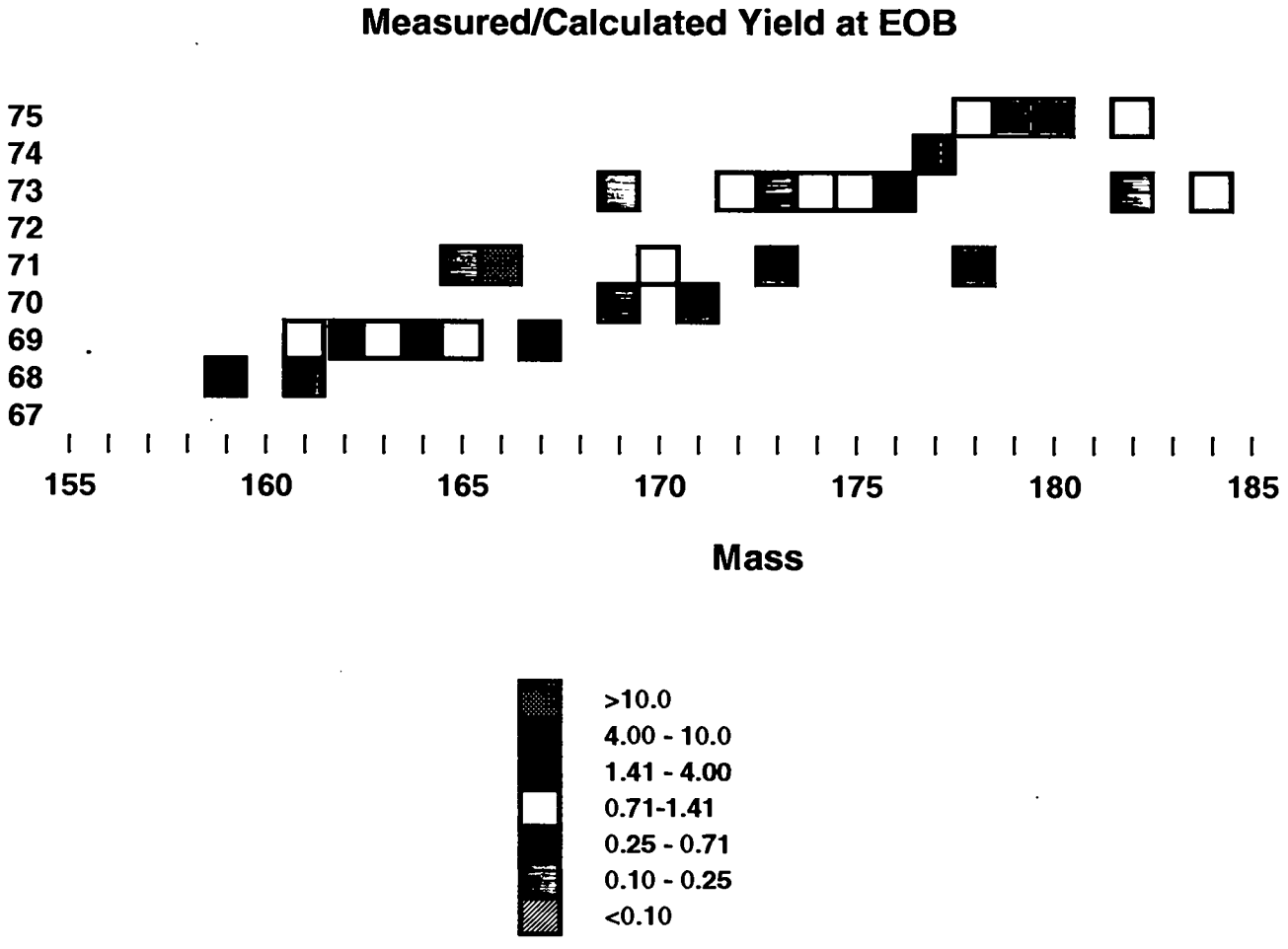

Fig. 14 Ratio of measured to calculated yields for radioisotopes identified in this experiment.

Table 3A Tungsten Yields at End of Bombardment
Six-second Irradiation

Nucleus	Z	Half-life (Sec)	Foil	Calculated ($N/cm^3/p$)	This Measurement ($N/cm^3/p$)	uncertainty	
161Tm	69	2280	425	7.51E-05	9.48E-05	8.14E-06	
162Tm	69	1302	425	6.07E-05	2.43E-04	9.60E-06	
164Tm	69	306	425	5.46E-05	2.20E-04	1.35E-05	
165Lu	71	644.4	425	1.13E-04	1.78E-05	2.49E-06	
166Lu	71	84.6	425	4.82E-05	1.47E-04	5.32E-05	
178Lu	71	1386	425	3.54E-06	8.81E-06	2.56E-06	
169Ta	73	294	425	1.17E-04	2.33E-05	1.05E-06	*
172Ta	73	2220	425	1.57E-04	1.32E-04	7.42E-06	
174W	74	1764	425	2.01E-04	1.48E-05	1.59E-06	*
178Re	75	792	425	6.09E-05	6.30E-05	2.37E-06	
179Re	75	1170	425	6.95E-05	1.08E-04	4.64E-06	
180Re	75	146.4	425	6.46E-05	9.93E-05	7.29E-06	

* Absolute branching ratio not tabulated.

Table 3B Tungsten Yields at End of Bombardment
One-hour Irradiation

Nucleus	Z	Half-life (sec)	Foil	Calculated (N/cm3/p)	This Measurement (c/cm3/p)	Uncertainty
147Gd	64	1.37E+05	614	5.95E-05	8.87E-06	6.92E-07
149Gd	64	8.12E+05	614	1.92E-05	5.46E-05	5.41E-06
166Ho	67	3.79E+08	614	0.00E+00	5.71E-01	3.22E-02
161Er	68	1.16E+04	614r	6.91E-05	1.00E-04	3.80E-07
163Tm	69	6.52E+03	614r	1.34E-04	6.83E-09	1.36E-06
165Tm	69	1.08E+05	614	1.45E-04	2.01E-04	9.20E-06
167Tm	69	7.98E+05	614	5.78E-05	2.51E-04	1.80E-05
169Lu	71	1.23E+05	614	2.68E-04	1.88E-04	1.25E-06
167Lu	71	3.09E+03	614	1.83E-04	4.12E-05	6.38E-06
170Hf	72	5.76E+04	614	2.51E-04	1.59E-04	1.47E-06
171Lu	71	7.12E+05	614	3.53E-05	3.27E-04	3.84E-06
170Hf	72	5.76E+04	614r	2.51E-04	2.07E-04	2.65E-06
173Hf	72	8.50E+04	614	7.24E-05	2.48E-04	1.85E-06
173Ta	73	1.13E+04	614r	2.89E-04	1.84E-04	8.29E-07
174Ta	73	4.25E+03	614r	1.78E-04	2.13E-04	1.33E-06
175Ta	73	3.78E+04	614r	2.27E-04	2.50E-04	6.10E-06
176Ta	73	2.91E+04	614r	1.53E-04	2.35E-04	1.87E-06
182Ta	73	9.89E+06	614	6.03E-04	2.11E-04	8.99E-06
184Ta	73	3.13E+04	614r	3.02E-05	2.12E-05	2.86E-07
177W	74	8.10E+03	614r	7.82E-06	1.52E-04	6.30E-07
187W	74	8.60E+04	614r	7.56E-04	3.84E-04	5.52E-06
182Re	75	2.30E+05	614	1.29E-04	1.88E-05	1.19E-06

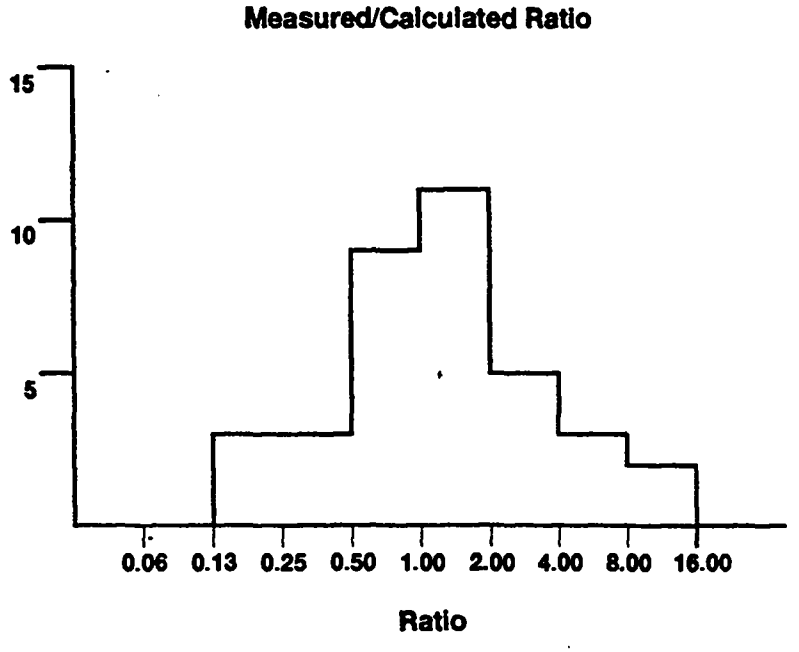

Fig. 15. Histogram of ratio of measured to calculated spallation yields for a foil at Position 4A in the W assembly.

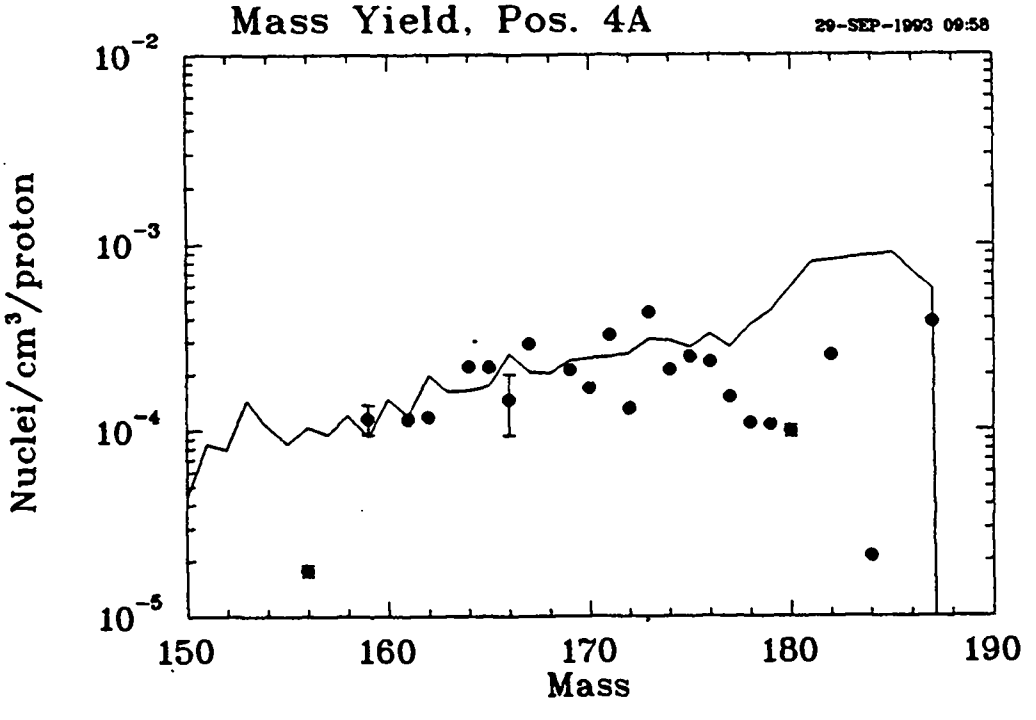

Fig 16. Mass yield at position 4A in the W assembly. The points are the measured values with statistical uncertainties. In most cases, the statistical uncertainty is smaller than the point. The curve is the calculation of Ref. 15, with stable isotopes deleted.

5. Discussion

The information provided in this report summarizes our progress to date in benchmarking the radionuclide production code package that is used in APT design and analysis. The experimental measurements were performed accurately and analysis of those data will provide valid information that will be invaluable in benchmarking spallation radionuclide production and the subsequent modification of those radionuclides through neutron interactions and decay. There was a vast quantity of data collected. Unfortunately, due to funding decreases in FY-1993, our ability to conduct analysis of the data was reduced severely. We concentrated on improving our computer analysis programs and their libraries, completing the necessary preanalysis checks on experimental procedure and data correction, such as detector energy calibration and efficiency determination, and then applying all of this to analysis of data from a single foil position. As discussed earlier, we analyzed data for our short and medium irradiations of on-axis foils from position 4A. The data presented here are the first to evaluate the production of short-half lived nuclei, and are also the first data of its kind for tungsten. The successful analysis of these data gives us great confidence that significant additional information will be extracted during FY-1994.

The summary information presented in Fig. 15 is the first indication of the accuracy with which the code packages calculate the radionuclide production. The present picture is far from complete, but the results are in qualitative agreement with pre-test indications - fifty-six percent of the radionuclide yields are computed within a factor of two, but that there is a broad distribution, and some radionuclides show more than a factor of ten disagreement with calculation. The comparison of measured to calculated mass yields, shown in Fig. 16, shows generally good agreement for masses below 176, but somewhat poorer agreement at larger masses. At this time we must defer definite conclusions. An additional correction to the calculated curve that would improve agreement would be to remove radionuclide production for masses that were definitely not observed. That will be done as soon as we have completed identification of all of the nuclei from position 4A and include the statistically more accurate results from the 8-hour long irradiation. In addition there remains analysis to extend the results on foil 4A to include weakly produced nuclei, nuclei with very long half-lives (mainly from analysis of the long irradiation results), two (or more)-component gamma peaks, and decays involving parent-daughter chains.

References

1. W. Amian, N.F. Peek, and D. Sterzenbach, "Production Rates of Spallation and Fission Products in Depleted Uranium and Natural Lead Targets Bombarded by 600 MeV and 1100 MeV Protons," Proceedings of the International Collaboration on Advanced Neutron Sources, ICANS-VII, September 13-16, 1983, Atomic Energy of Canada Limited, Report AECL-8488.

2. H. Takada, K. Hasegawa, T. Sasa, S. Meigo, and I. Kanno, "Integral Spallation Experiment with a Lead Assembly Irradiated with 500 MeV Protons," Proceedings of the 1992 Symposium on Nuclear Data, November 26-27, JAERI, Tokai, Japan, p72.
3. J.F. Breisneister, ed., "MCNP - A General Monte Carlo Code for Neutron and Photon Transport," LA-7396-M, Rev 2, Los Alamos National Laboratory, 1986.
4. T. Fukahori, S. Chiba, H. Takeda, N. Kishida, T. Watanabe, and N. Yamamuro, "Benchmark Calculations of Theoretical Calculation Codes for Nuclear Data Evaluations in the Intermediate Energy Region," Proceedings of the 1992 Symposium on Nuclear Data, November 26-27, JAERI, Tokai, Japan, p57.
5. N. P. Kocherov (Ed.), "Intermediate Energy Nuclear Data for Applications," Proceedings of the Advisory Group Meeting, International Atomic Energy Agency, 9-12 October, 1990, Vienna, Austria.
6. A. J. Koning, "Review of High Energy Data and Model Codes for Accelerator Based Transmutation for Accelerator Based Transmutation," NEA/NSC/Doc(92)12, June 1993.
7. A. J. Koning, "Requirements for an Evaluated Nuclear Data File for Accelerator Based Transmutation," NEA/NSC/Doc(93)6, June 1993.
8. R.E. Prael and H. Lichtenstein, "User Guide to LCS: The LAHET code System," Los Alamos National Laboratory, Sept. 15, 1989.
9. J.B. Cumming, et al., Nucl. Instr, and Meth. 180, 37 (1981).
10. Amersham QCD.1, Amersham Corp, Arlington Heights, IL.
11. R. Gunnink, computer code EFFIC (R. Gunnink, Fremont CA, 1991).
12. R. Gunnink and J.B. Niday, Computer code GAMANAL (Lawrence Livermore National Laboratory, Livermore CA, 1971. UCRL 51061. Modified for use at Los Alamos .
13. L. Spanier and P. Ekstrom, computer code GAMMAS (Dept. of Nuclear Physics, Lund University, Lund, Sweden, 1989).
14. W. Wilson, *et al.*,"Accelerator Transmutation Studies at Los Alamos with LAHET, MCNP, and CINDER'90," Los Alamos National Laboratory report LA-UR-93-3080.
15. W. Wilson, "Preliminary Results of Simulation Calculations of Tungsten Activation Experiments," Los Alamos National Laboratory Memorandum, T-2-M:93-3615.

Input Deck for LAHET Calculations

```
APT 800 MeV Pb tgt. LAHET deck.
Shower Test

300000,1,4,0,5000000,800000000,0,0,0,0023,0,0,0,1/
1,0,1,1,0,1,0,0,1,0 /
1,0,1,1,1,0,1,1/
0,0,0,0,0,1,1,1,1,1,1,1,1,1,1,1,1/
1,1,0,0,0,0,0,0,0,1/
1000.,.1,20.,0.,0.,-1,0,1,1,-1,1.5,8.0,1.5,14,0
.0,2,0
7,14,.00003349,0
8,16,.00000945,0
.0,5,0
74,180,.000082,0
74,182,.016621,0
74,183,.009037,0
74,184,.019382,0
74,186,.018074,0
.0,4,0
82,204,.000470,0
82,206,.007975,0
82,207,.007313,0
82,208,.017340,0
.000376,2,0
6,12,.005614,0
8,16,.001535,0
  1  1 -.00103 18 -19 24 -25 1 -3
  2  0       -22 21 24 -28 2 -3
  3  3 -11.39  23 -22 26 -28 1 -3 #1 #2
  4  3 -11.39  20 -21 26 -27 (-18:-24) 3 -4
  5  4 -1.000  18 -21 24 -27 29 31 33 35 37 3 -39
  6  1 -.00103 (-29:-31:-33:-35:-37) 3 -39
  7  4 -1.000  18 -21 24 -27 30 32 34 36 38 39 39 -40
  8  2 -19.3   -30              39 -40
  9  2 -19.3      -32           39 -40
 10  2 -19.3         -34        39 -40
 11  2 -19.3            -36     39 -40
 12  2 -19.3               -38  39 -40
 13  4 -1.00   18 -21 24 -27 40 -41
 14  1 -.00103 18 -21 24 -27 41 -4
```

```
15  2 -19.3  20 -21 26 -27 4 -5
16  3 -11.39  20 -21 26 -27 (-18:-24) 5 -6
17  4 -1.000  18 -21 24 -27 29 31 33 35 37 5 -42
18  1 -.00103 (-29:-31:-33:-35:-37) 5 -42
19  4 -1.000  18 -21 24 -27 30 32 34 36 38 39 42 -43
20  2 -19.3  -30              42 -43
21  2 -19.3     -32           42 -43
22  2 -19.3        -34        42 -43
23  2 -19.3           -36     42 -43
24  2 -19.3              -38  42 -43
25  4 -1.00  18 -21 24 -27 43 -44
26  1 -.00103 18 -21 24 -27 44 -6
27  2 -19.3  20 -21 26 -27 6 -7
28  3 -11.39  20 -21 26 -27 (-18:-24) 7 -8
29  4 -1.000  18 -21 24 -27 29 31 33 35 37 7 -45
30  1 -.00103 (-29:-31:-33:-35:-37) 7 -45
31  4 -1.000  18 -21 24 -27 30 32 34 36 38 39 45 -46
32  2 -19.3  -30              45 -46
33  2 -19.3     -32           45 -46
34  2 -19.3        -34        45 -46
35  2 -19.3           -36     45 -46
36  2 -19.3              -38  45 -46
37  4 -1.00  18 -21 24 -27 46 -47
38  1 -.00103 18 -21 24 -27 47 -8
39  2 -19.3  20 -21 26 -27 8 -9
40  3 -11.39  20 -21 26 -27 (-18:-24) 9 -10
41  4 -1.000  18 -21 24 -27 29 31 33 35 37 9 -48
42  1 -.00103 (-29:-31:-33:-35:-37) 9 -48
43  4 -1.000  18 -21 24 -27 30 32 34 36 38 39 48 -49
44  2 -19.3  -30              48 -49
45  2 -19.3     -32           48 -49
46  2 -19.3        -34        48 -49
47  2 -19.3           -36     48 -49
48  2 -19.3              -38  48 -49
49  4 -1.00  18 -21 24 -27 49 -50
50  1 -.00103 18 -21 24 -27 50 -10
51  2 -19.3  20 -21 26 -27 10 -11
52  3 -11.39  20 -21 26 -27 (-18:-24) 11 -12
53  4 -1.000  18 -21 24 -27 29 31 33 35 37 11 -51
54  1 -.00103 (-29:-31:-33:-35:-37) 11 -51
55  4 -1.000  18 -21 24 -27 30 32 34 36 38 39 51 -52
56  2 -19.3  -30              51 -52
57  2 -19.3     -32           51 -52
58  2 -19.3        -34        51 -52
```

```
 59  2 -19.3          -36    51 -52
 60  2 -19.3             -38 51 -52
 61  4 -1.00  18 -21 24 -27 52 -53
 62  1 -.00103 18 -21 24 -27 53 -12
 63  2 -19.3  20 -21 26 -27 12 -13
 64  3 -11.39 20 -21 26 -27 (-18:-24) 13 -14
 65  4 -1.000 18 -21 24 -27 29 31 33 35 37 13 -54
 66  1 -.00103 (-29:-31:-33:-35:-37) 13 -54
 67  4 -1.000 18 -21 24 -27 30 32 34 36 38 39 54 -55
 68  2 -19.3  -30           54 -55
 69  2 -19.3     -32        54 -55
 70  2 -19.3        -34     54 -55
 71  2 -19.3           -36  54 -55
 72  2 -19.3             -38 54 -55
 73  4 -1.00  18 -21 24 -27 55 -56
 74  1 -.00103 18 -21 24 -27 56 -14
 75  2 -19.3  20 -21 26 -27 14 -15
 76  3 -11.39 20 -21 26 -27 (-18:-24) 15 -16
 77  4 -1.000 18 -21 24 -27 29 31 33 35 37 15 -57
 78  1 -.00103 (-29:-31:-33:-35:-37) 15 -57
 79  4 -1.000 18 -21 24 -27 30 32 34 36 38 39 57 -58
 80  2 -19.3  -30           57 -58
 81  2 -19.3     -32        57 -58
 82  2 -19.3        -34     57 -58
 83  2 -19.3           -36  57 -58
 84  2 -19.3             -38 57 -58
 85  4 -1.00  18 -21 24 -27 58 -59
 86  1 -.00103 18 -21 24 -27 59 -16
 87  2 -19.3  20 -21 26 -27 16 -17
 88  3 -11.39 20 -21 26 -27 (-18:-24) 17 -63
 89  4 -1.000 18 -21 24 -27 29 31 33 35 37 17 -60
 90  1 -.00103 (-29:-31:-33:-35:-37) 17 -60
 91  4 -1.000 18 -21 24 -27 30 32 34 36 38 39 60 -61
 92  2 -19.3  -30           60 -61
 93  2 -19.3     -32        60 -61
 94  2 -19.3        -34     60 -61
 95  2 -19.3           -36  60 -61
 96  2 -19.3             -38 60 -61
 97  4 -1.00  18 -21 24 -27 61 -62
 98  1 -.00103 18 -21 24 -27 62 -63
 99  2 -19.3  20 -21 26 -27 63 -64
100  0       -1:64:-26:28:-23:22:(3 21):(3 -20):(3 -26):(3 27)

  1 pz 0.000
```

```
 2 pz 17.78
 3 pz 20.32
 4 pz 20.955
 5 pz 26.035
 6 pz 26.67
 7 pz 31.75
 8 pz 32.385
 9 pz 37.465
10 pz 38.10
11 pz 43.18
12 pz 43.815
13 pz 48.895
14 pz 49.53
15 pz 54.61
16 pz 55.245
17 pz 60.325
18 px -2.54
19 px 2.54
20 px -10.16
21 px 10.16
22 px 15.24
23 px -15.24
24 py -2.54
25 py 2.54
26 py -10.16
27 py 10.16
28 py 15.24
29 cz  0.794
30 cz  1.032
31 c/z 2.144 2.144 0.794
32 c/z 2.144 2.144 1.032
33 c/z 4.285  4.285 0.794
34 c/z 4.285  4.285 1.032
35 c/z 6.429  6.429 0.794
36 c/z 6.429  6.429 1.032
37 c/z 8.573  8.573 0.794
38 c/z 8.573  8.573 1.032
39 pz 20.409
40 pz 20.638
41 pz 20.796
42 pz 26.124
43 pz 26.353
44 pz 26.511
45 pz 31.839
```

46 pz 32.068
47 pz 32.226
48 pz 37.554
49 pz 37.783
50 pz 37.941
51 pz 43.269
52 pz 43.498
53 pz 43.656
54 pz 48.984
55 pz 49.213
56 pz 49.371
57 pz 54.699
58 pz 54.928
59 pz 55.086
60 pz 60.414
61 pz 60.643
62 pz 60.801
63 pz 60.96
64 pz 66.04

in 1 98r 0

2,800.,0.,0.00001,0.4,0.2,2.00/

Input Deck for MCNP Calculations

```
c  W target for APT target source expt. MCNP deck.
  1  1 -.00103 18 -19 24 -25 1 -3
  2  0       -22 21 24 -28 2 -3
  3  3 -11.39  23 -22 26 -28 1 -3 #1 #2
  4  3 -11.39  20 -21 26 -27 (-18:-24) 3 -4
  5  4 -1.000  18 -21 24 -27 29 31 33 35 37 3 -39
  6  1 -.00103 (-29:-31:-33:-35:-37) 3 -39
  7  4 -1.000  18 -21 24 -27 30 32 34 36 38 39 39 -40
  8  2 -19.3   -30              39 -40
  9  2 -19.3      -32           39 -40
 10  2 -19.3         -34        39 -40
 11  2 -19.3            -36     39 -40
 12  2 -19.3               -38  39 -40
 13  4 -1.00   18 -21 24 -27 40 -41
 14  1 -.00103 18 -21 24 -27 41 -4
 15  2 -19.3   20 -21 26 -27 4 -5
 16  3 -11.39  20 -21 26 -27 (-18:-24) 5 -6
 17  4 -1.000  18 -21 24 -27 29 31 33 35 37 5 -42
 18  1 -.00103 (-29:-31:-33:-35:-37) 5 -42
 19  4 -1.000  18 -21 24 -27 30 32 34 36 38 39 42 -43
 20  2 -19.3   -30              42 -43
 21  2 -19.3      -32           42 -43
 22  2 -19.3         -34        42 -43
 23  2 -19.3            -36     42 -43
 24  2 -19.3               -38  42 -43
 25  4 -1.00   18 -21 24 -27 43 -44
 26  1 -.00103 18 -21 24 -27 44 -6
 27  2 -19.3   20 -21 26 -27 6 -7
 28  3 -11.39  20 -21 26 -27 (-18:-24) 7 -8
 29  4 -1.000  18 -21 24 -27 29 31 33 35 37 7 -45
 30  1 -.00103 (-29:-31:-33:-35:-37) 7 -45
 31  4 -1.000  18 -21 24 -27 30 32 34 36 38 39 45 -46
 32  2 -19.3   -30              45 -46
 33  2 -19.3      -32           45 -46
 34  2 -19.3         -34        45 -46
 35  2 -19.3            -36     45 -46
 36  2 -19.3               -38  45 -46
 37  4 -1.00   18 -21 24 -27 46 -47
 38  1 -.00103 18 -21 24 -27 47 -8
 39  2 -19.3   20 -21 26 -27 8 -9
 40  3 -11.39  20 -21 26 -27 (-18:-24) 9 -10
```

```
41  4 -1.000  18 -21 24 -27 29 31 33 35 37 9 -48
42  1 -.00103 (-29:-31:-33:-35:-37) 9 -48
43  4 -1.000  18 -21 24 -27 30 32 34 36 38 39 48 -49
44  2 -19.3   -30              48 -49
45  2 -19.3     -32            48 -49
46  2 -19.3       -34          48 -49
47  2 -19.3         -36        48 -49
48  2 -19.3           -38      48 -49
49  4 -1.00   18 -21 24 -27 49 -50
50  1 -.00103 18 -21 24 -27 50 -10
51  2 -19.3   20 -21 26 -27 10 -11
52  3 -11.39  20 -21 26 -27 (-18:-24) 11 -12
53  4 -1.000  18 -21 24 -27 29 31 33 35 37 11 -51
54  1 -.00103 (-29:-31:-33:-35:-37) 11 -51
55  4 -1.000  18 -21 24 -27 30 32 34 36 38 39 51 -52
56  2 -19.3   -30              51 -52
57  2 -19.3     -32            51 -52
58  2 -19.3       -34          51 -52
59  2 -19.3         -36        51 -52
60  2 -19.3           -38      51 -52
61  4 -1.00   18 -21 24 -27 52 -53
62  1 -.00103 18 -21 24 -27 53 -12
63  2 -19.3   20 -21 26 -27 12 -13
64  3 -11.39  20 -21 26 -27 (-18:-24) 13 -14
65  4 -1.000  18 -21 24 -27 29 31 33 35 37 13 -54
66  1 -.00103 (-29:-31:-33:-35:-37) 13 -54
67  4 -1.000  18 -21 24 -27 30 32 34 36 38 39 54 -55
68  2 -19.3   -30              54 -55
69  2 -19.3     -32            54 -55
70  2 -19.3       -34          54 -55
71  2 -19.3         -36        54 -55
72  2 -19.3           -38      54 -55
73  4 -1.00   18 -21 24 -27 55 -56
74  1 -.00103 18 -21 24 -27 56 -14
75  2 -19.3   20 -21 26 -27 14 -15
76  3 -11.39  20 -21 26 -27 (-18:-24) 15 -16
77  4 -1.000  18 -21 24 -27 29 31 33 35 37 15 -57
78  1 -.00103 (-29:-31:-33:-35:-37) 15 -57
79  4 -1.000  18 -21 24 -27 30 32 34 36 38 39 57 -58
80  2 -19.3   -30              57 -58
81  2 -19.3     -32            57 -58
82  2 -19.3       -34          57 -58
83  2 -19.3         -36        57 -58
84  2 -19.3           -38      57 -58
```

```
 28 py 15.24
 29 cz  0.794
 30 cz  1.032
 31 c/z 2.144 2.144 0.794
 32 c/z 2.144 2.144 1.032
 33 c/z 4.285  4.285 0.794
 34 c/z 4.285  4.285 1.032
 35 c/z 6.429  6.429 0.794
 36 c/z 6.429  6.429 1.032
 37 c/z 8.573  8.573 0.794
 38 c/z 8.573  8.573 1.032
 39 pz 20.409
 40 pz 20.638
 41 pz 20.796
 42 pz 26.124
 43 pz 26.353
 44 pz 26.511
 45 pz 31.839
 46 pz 32.068
 47 pz 32.226
 48 pz 37.554
 49 pz 37.783
 50 pz 37.941
 51 pz 43.269
 52 pz 43.498
 53 pz 43.656
 54 pz 48.984
 55 pz 49.213
 56 pz 49.371
 57 pz 54.699
 58 pz 54.928
 59 pz 55.086
 60 pz 60.414
 61 pz 60.643
 62 pz 60.801
 63 pz 60.96
 64 pz 66.04

imp:n  1 98r 0
files 77 neutp s u 0 78 neutpa s u 0 70 histx s u 0
mode   n
f4:n            8 20 32 44 56 68
e4    1.0e-11 5.0e-9 1.0e-8 1.5e-8 2.0e-8 2.5e-8 3.0e-8 3.5e-8 4.2e-8
    5.0e-8 5.8e-8 6.7e-8 8.0e-8 1.0e-7 1.52e-7 2.51e-7 4.14e-7
```

```
   6.83e-7 1.125e-6 1.1855e-6 3.059e-6 5.043e-6 8.315e-6 1.371e-5
   2.26e-5 3.727e-5 6.144e-5 1.013e-4 1.67e-4 2.754e-4 4.54e-4 7.485e-4
   1.234e-3 2.035e-3 2.404e-3 2.840e-3 3.355e-3 5.531e-3 9.119e-3
   1.503e-2 1.989e-2 2.554e-2 4.087e-2 6.738e-2 1.111e-1 1.832e-1
   3.02e-1 3.887e-1 4.979e-1 .639279 .82085 1.10803 1.35335 1.73774
   2.2313 2.86505 3.67879 4.96585 6.06510 10.0 14.9182 16.9046 20.0 25.0
fm4 6.25e11
m1  7014.50c -.78 8016.50c -.22
m2  74000.55c 1.0
m3  82000.50c 1.0
m4  6000.50c -.746 1001.50c -.05 8016.50c -.204
phys:n 20.
```

Table B-1
Caculated mass yield for 800 MeV protons on Tungsten at Position 4A
1.63 x 10^{12} protons over 6 sec Irradiation
Calculated with CINDER'90 using 5/93 Library for indicated decay times.

Nuclide	Halflife sec	Yield EOB	Yield T(1) (394.5 sec) n/cm^3/p	Yield T(2) (2185 sec) n/cm^3/p	Yield T(3) (3976 sec) n/cm^3/p
H___3	3.89E+08	4.95E-08	4.95E-08	4.95E-08	4.95E-08
S__37	3.03E+02	4.33E-06	1.76E-06	2.92E-08	4.86E-10
Ar_43	3.22E+02	4.33E-06	1.85E-06	3.92E-08	8.31E-10
Sc_44	1.41E+04	4.36E-06	4.27E-06	3.91E-06	3.59E-06
Sc_47	2.89E+05	4.36E-06	4.35E-06	4.33E-06	4.32E-06
Sc_48	1.57E+05	4.36E-06	4.35E-06	4.32E-06	4.28E-06
Co_60	1.66E+08	4.36E-06	4.36E-06	4.36E-06	4.36E-06
Cu_66	3.06E+02	4.33E-06	1.77E-06	3.07E-08	5.31E-10
Zn_72	1.67E+05	4.36E-06	4.35E-06	4.32E-06	4.29E-06
Ga_66	3.42E+04	4.36E-06	4.32E-06	4.17E-06	4.02E-06
Ga_67	2.82E+05	4.36E-06	4.35E-06	4.33E-06	4.31E-06
Ge_69	1.41E+05	4.36E-06	4.35E-06	4.31E-06	4.27E-06
As_74	1.54E+06	4.36E-06	4.36E-06	4.35E-06	4.35E-06
As_77	1.40E+05	4.36E-06	4.35E-06	4.31E-06	4.27E-06
Se_73	2.57E+04	4.36E-06	4.31E-06	4.11E-06	3.91E-06
Br_78	3.88E+02	1.30E-05	6.42E-06	2.61E-07	1.06E-08
Br_83	8.64E+03	4.36E-06	4.22E-06	3.66E-06	3.17E-06
Kr_79	1.26E+05	4.36E-06	4.35E-06	4.31E-06	4.26E-06
Kr_81	6.72E+12	4.36E-06	4.36E-06	4.36E-06	4.36E-06
Rb_81	1.65E+04	4.36E-06	4.28E-06	3.97E-06	3.69E-06
Rb_84	2.84E+06	4.36E-06	4.36E-06	4.35E-06	4.35E-06
Sr_85	5.60E+06	4.36E-06	4.36E-06	4.36E-06	4.36E-06
Y__87	2.89E+05	4.36E-06	4.35E-06	4.33E-06	4.32E-06
Y__88	9.22E+06	4.36E-06	4.36E-06	4.36E-06	4.36E-06
Zr_86	5.94E+04	4.36E-06	4.34E-06	4.25E-06	4.16E-06
Zr_98	3.07E+01	4.08E-06	5.52E-10	1.53E-27	4.25E-45
Nb_90	5.26E+04	4.36E-06	4.33E-06	4.23E-06	4.13E-06
Nb_95	3.02E+06	4.36E-06	4.36E-06	4.36E-06	4.35E-06
Nb_97	4.33E+03	4.36E-06	4.09E-06	3.07E-06	2.30E-06
Te116	8.96E+03	4.36E-06	4.23E-06	3.68E-06	3.20E-06
Te118	5.18E+05	4.36E-06	4.35E-06	4.34E-06	4.33E-06
I_121	7.63E+03	4.36E-06	4.20E-06	3.57E-06	3.04E-06
Ba127	7.62E+02	4.35E-06	3.04E-06	5.95E-07	1.17E-07
Ba131	1.02E+06	4.36E-06	4.36E-06	4.35E-06	4.35E-06
La131	3.54E+03	4.35E-06	4.03E-06	2.84E-06	2.00E-06
La133	1.41E+04	4.36E-06	4.27E-06	3.91E-06	3.58E-06
La135	7.02E+04	4.36E-06	4.34E-06	4.26E-06	4.19E-06
Ce131	6.00E+02	4.34E-06	2.75E-06	3.48E-07	4.40E-08
Ce132	1.26E+04	1.31E-05	1.28E-05	1.16E-05	1.05E-05
Ce134	2.73E+05	4.36E-06	4.35E-06	4.33E-06	4.31E-06

Ce135	6.37E+04	8.71E-06	8.68E-06	8.51E-06	8.35E-06
Pr136	7.86E+02	4.35E-06	3.07E-06	6.33E-07	1.30E-07
Pr137	4.61E+03	8.71E-06	8.21E-06	6.27E-06	4.79E-06
Nd136	3.04E+03	4.35E-06	3.98E-06	2.65E-06	1.76E-06
Nd137	2.31E+03	8.71E-06	7.73E-06	4.52E-06	2.64E-06
Nd138	1.81E+04	1.31E-05	1.29E-05	1.20E-05	1.12E-05
Nd139	1.78E+03	1.31E-05	1.12E-05	5.58E-06	2.78E-06
Nd140	2.91E+05	1.31E-05	1.31E-05	1.30E-05	1.29E-05
Pm139	2.49E+02	4.32E-06	1.44E-06	9.86E-09	6.75E-11
Pm140	9.20E+00	1.75E-05	2.16E-18	5.61E-77	
Pm141	1.25E+03	8.70E-06	7.00E-06	2.60E-06	9.66E-07
Pm142	4.05E+01	1.66E-05	1.94E-08	9.52E-22	4.68E-35
Pm143	2.29E+07	8.71E-06	8.71E-06	8.71E-06	8.71E-06
Pm145	5.59E+08	4.36E-06	4.36E-06	4.36E-06	4.36E-06
Pm149	1.91E+05	4.36E-06	4.35E-06	4.32E-06	4.29E-06
Sm138	1.80E+02	4.31E-06	9.43E-07	9.55E-10	9.67E-13
Sm140	8.89E+02	4.35E-06	3.20E-06	7.91E-07	1.96E-07
Sm141	6.12E+02	1.30E-05	8.33E-06	1.10E-06	1.44E-07
Sm142	4.35E+03	3.92E-05	3.68E-05	2.77E-05	2.08E-05
Sm143	5.30E+02	2.17E-05	1.30E-05	1.24E-06	1.20E-07
Sm145	2.94E+07	4.36E-06	4.36E-06	4.36E-06	4.36E-06
Eu142	2.40E+00	2.07E-06	6.83E-56		
Eu143	1.58E+02	1.29E-05	2.29E-06	8.86E-10	3.44E-13
Eu144	1.02E+01	2.86E-05	6.52E-17	9.36E-70	
Eu145	5.12E+05	5.23E-05	5.23E-05	5.21E-05	5.20E-05
Eu146	3.97E+05	1.74E-05	1.74E-05	1.74E-05	1.73E-05
Eu147	2.07E+06	2.61E-05	2.61E-05	2.61E-05	2.61E-05
Gd145	1.38E+03	8.70E-06	7.14E-06	2.90E-06	1.18E-06
Gd146	4.17E+06	2.61E-05	2.61E-05	2.61E-05	2.61E-05
Gd147	1.37E+05	5.23E-05	5.22E-05	5.17E-05	5.12E-05
Gd148	2.35E+09	3.05E-05	3.05E-05	3.05E-05	3.05E-05
Gd149	8.10E+05	1.74E-05	1.74E-05	1.74E-05	1.74E-05
Gd150	5.65E+13	8.71E-06	8.71E-06	8.71E-06	8.71E-06
Gd151	1.07E+07	8.71E-06	8.71E-06	8.71E-06	8.71E-06
Gd153	2.09E+07	4.36E-06	4.36E-06	4.36E-06	4.36E-06
Tb146	8.00E+00	3.40E-06	4.86E-21	2.05E-88	
Tb147	5.90E+03	2.61E-05	2.50E-05	2.02E-05	1.64E-05
Tb148	3.60E+03	4.35E-06	4.04E-06	2.86E-06	2.03E-06
Tb149	1.49E+04	2.18E-05	2.14E-05	1.97E-05	1.81E-05
Tb150	1.25E+04	2.61E-05	2.56E-05	2.32E-05	2.10E-05
Tb151	6.34E+04	3.92E-05	3.90E-05	3.83E-05	3.75E-05
Tb152	6.30E+04	1.74E-05	1.74E-05	1.70E-05	1.67E-05
Tb153	2.02E+05	2.61E-05	2.61E-05	2.59E-05	2.58E-05
Tb154	7.74E+04	4.36E-06	4.34E-06	4.27E-06	4.20E-06
Tb157	4.73E+09	4.36E-06	4.36E-06	4.36E-06	4.36E-06
Dy148	1.86E+02	1.72E-05	3.96E-06	5.01E-09	6.34E-12
Dy149	2.54E+02	1.73E-05	5.89E-06	4.45E-08	3.36E-10
Dy150	4.30E+02	3.04E-05	1.61E-05	8.98E-07	5.02E-08
Dy151	1.07E+03	3.91E-05	3.03E-05	9.55E-06	3.01E-06
Dy152	8.57E+03	6.53E-05	6.33E-05	5.48E-05	4.74E-05
Dy153	2.30E+04	6.97E-05	6.89E-05	6.53E-05	6.18E-05
Dy154	9.47E+13	3.49E-05	3.49E-05	3.49E-05	3.49E-05

Dy155	3.60E+04	1.31E-05	1.30E-05	1.25E-05	1.21E-05
Dy157	2.93E+04	4.36E-06	4.32E-06	4.14E-06	3.97E-06
Dy159	1.25E+07	4.36E-06	4.36E-06	4.36E-06	4.36E-06
Ho150	2.60E+01	4.03E-06	1.09E-10	2.03E-31	3.77E-52
Ho151	3.52E+01	1.64E-05	6.95E-09	3.39E-24	1.65E-39
Ho152	1.62E+02	2.58E-05	4.76E-06	2.22E-09	1.04E-12
Ho153	1.20E+02	7.28E-05	7.46E-06	2.40E-10	7.75E-15
Ho154	7.10E+02	3.91E-05	2.66E-05	4.63E-06	8.07E-07
Ho155	2.88E+03	4.35E-05	3.96E-05	2.57E-05	1.67E-05
Ho156	3.36E+03	4.79E-05	4.42E-05	3.05E-05	2.11E-05
Ho157	7.56E+02	8.69E-06	6.05E-06	1.17E-06	2.27E-07
Ho158	6.78E+02	4.34E-06	2.90E-06	4.65E-07	7.46E-08
Ho159	1.98E+03	4.35E-06	3.79E-06	2.03E-06	1.08E-06
Ho160	1.54E+03	4.35E-06	3.64E-06	1.62E-06	7.24E-07
Ho163	1.44E+11	1.31E-05	1.31E-05	1.31E-05	1.31E-05
Er152	1.03E+01	3.58E-06	1.06E-17	4.96E-70	
Er153	3.71E+01	2.06E-05	1.30E-08	3.85E-23	1.14E-37
Er154	2.21E+02	6.04E-05	1.75E-05	6.38E-08	2.32E-10
Er155	3.18E+02	5.63E-05	2.38E-05	4.81E-07	9.70E-09
Er156	1.17E+03	6.09E-05	4.82E-05	1.67E-05	5.78E-06
Er157	1.12E+03	6.09E-05	4.77E-05	1.57E-05	5.19E-06
Er158	8.10E+03	8.71E-05	8.42E-05	7.23E-05	6.20E-05
Er159	2.16E+03	2.18E-05	1.92E-05	1.08E-05	6.08E-06
Er160	1.03E+05	4.79E-05	4.78E-05	4.72E-05	4.67E-05
Er161	1.16E+04	1.31E-05	1.28E-05	1.15E-05	1.03E-05
Tm155	3.40E+01	8.20E-06	2.64E-09	3.70E-25	5.20E-41
Tm156	8.38E+01	8.50E-06	3.25E-07	1.20E-13	4.45E-20
Tm157	2.10E+02	4.75E-05	1.29E-05	3.50E-08	9.50E-11
Tm158	2.41E+02	4.32E-05	1.39E-05	8.06E-08	4.67E-10
Tm159	5.46E+02	6.08E-05	3.68E-05	3.79E-06	3.91E-07
Tm160	5.64E+02	6.08E-05	3.74E-05	4.15E-06	4.59E-07
Tm161	1.98E+03	6.53E-05	5.69E-05	3.04E-05	1.62E-05
Tm162	1.30E+03	6.09E-05	4.94E-05	1.90E-05	7.34E-06
Tm163	6.52E+03	4.79E-05	4.59E-05	3.80E-05	3.14E-05
Tm164	1.20E+02	2.14E-05	2.19E-06	7.07E-11	2.28E-15
Tm165	1.08E+05	2.61E-05	2.61E-05	2.58E-05	2.55E-05
Tm166	2.77E+04	4.36E-06	4.31E-06	4.13E-06	3.94E-06
Tm167	7.99E+05	4.36E-06	4.36E-06	4.35E-06	4.34E-06
Tm171	6.06E+07	4.36E-06	4.36E-06	4.36E-06	4.36E-06
Tm173	2.97E+04	4.36E-06	4.32E-06	4.14E-06	3.97E-06
Yb157	3.86E+01	8.26E-06	6.93E-09	7.53E-23	8.19E-37
Yb158	9.40E+01	1.70E-05	9.30E-07	1.72E-12	3.16E-18
Yb159	8.40E+01	2.98E-05	1.15E-06	4.40E-13	1.69E-19
Yb160	2.88E+02	6.92E-05	2.68E-05	3.60E-07	4.84E-09
Yb161	2.52E+02	6.48E-05	2.19E-05	1.59E-07	1.16E-09
Yb162	1.13E+03	1.35E-04	1.06E-04	3.54E-05	1.18E-05
Yb163	6.63E+02	4.34E-05	2.88E-05	4.42E-06	6.80E-07
Yb164	4.55E+03	6.10E-05	5.74E-05	4.37E-05	3.33E-05
Yb165	5.94E+02	2.61E-05	1.64E-05	2.03E-06	2.52E-07
Yb166	2.04E+05	3.92E-05	3.92E-05	3.89E-05	3.87E-05
Yb167	1.05E+03	2.17E-05	1.68E-05	5.14E-06	1.58E-06
Yb169	2.77E+06	2.18E-05	2.18E-05	2.18E-05	2.18E-05

Table B-2
Caculated mass yield for 800 MeV protons on Tungsten at Position 4A
3.31×10^{14} protons over 1.1 hr Irradiation
Calculated with CINDER'90 using 5/93 Library for indicated decay times.

Nuclide		Halflife (Sec)	Yield EOB n/cm3/p	Yield T(1) 2.3 h n/cm3/p	Yield T(2) 3.4 h n/cm3/p	Yield T(3) 4.5h n/cm3/p
H	3	3.89E+08	4.94E-08	4.94E-08	4.94E-08	4.94E-08
Ne	25	6.02E-01	9.65E-10	0.00E+00	0.00E+00	0.00E+00
Na	25	5.96E+01	9.57E-08	1.10E-48	6.97E-69	4.42E-89
S	37	3.03E+02	4.86E-07	4.31E-15	4.57E-19	4.88E-23
Ar	43	3.22E+02	5.17E-07	1.37E-14	2.49E-18	4.57E-22
K	43	8.03E+04	3.76E-06	3.53E-06	3.41E-06	3.29E-06
Sc	44	1.41E+04	3.96E-06	2.66E-06	2.18E-06	1.79E-06
Sc	47	2.89E+05	4.34E-06	4.25E-06	4.19E-06	4.16E-06
Sc	48	1.57E+05	4.31E-06	4.16E-06	4.08E-06	4.02E-06
Co	60	1.66E+08	4.34E-06	4.34E-06	4.34E-06	4.34E-06
Ni	71	5.00E-01	8.03E-10	0.00E+00	0.00E+00	0.00E+00
Cu	66	3.06E+02	4.91E-07	5.20E-15	6.07E-19	7.05E-23
Cu	71	2.00E+01	3.21E-08	0.00E+00	0.00E+00	0.00E+00
Zn	71	1.47E+02	2.36E-07	5.95E-24	3.84E-32	2.49E-40
Zn	72	1.67E+05	4.31E-06	4.16E-06	4.10E-06	4.05E-06
Ga	66	3.42E+04	4.19E-06	3.55E-06	3.27E-06	3.01E-06
Ga	67	2.82E+05	4.34E-06	4.25E-06	4.19E-06	4.16E-06
Ge	69	1.41E+05	4.31E-06	4.13E-06	4.05E-06	3.99E-06
As	74	1.54E+06	4.34E-06	4.34E-06	4.31E-06	4.31E-06
As	77	1.40E+05	4.31E-06	4.13E-06	4.05E-06	3.96E-06
Se	73	2.57E+04	4.13E-06	3.32E-06	2.98E-06	2.67E-06
Br	78	3.88E+02	1.86E-06	9.45E-13	7.40E-16	5.81E-19
Br	83	8.64E+03	3.73E-06	1.95E-06	1.41E-06	1.03E-06
Kr	79	1.26E+05	4.31E-06	4.10E-06	4.02E-06	3.93E-06
Kr	81	6.72E+12	4.34E-06	4.34E-06	4.34E-06	4.34E-06
Rb	81	1.65E+04	4.02E-06	2.85E-06	2.41E-06	2.03E-06
Rb	84	2.84E+06	4.34E-06	4.34E-06	4.34E-06	4.34E-06
Sr	85	5.60E+06	4.34E-06	4.34E-06	4.34E-06	4.34E-06
Y	87	2.89E+05	4.34E-06	4.25E-06	4.19E-06	4.16E-06
Y	88	9.22E+06	4.34E-06	4.34E-06	4.34E-06	4.34E-06
Zr	86	5.94E+04	4.25E-06	3.87E-06	3.70E-06	3.53E-06
Zr	98	3.07E+01	4.91E-08	1.64E-87	0.00E+00	0.00E+00
Nb	90	5.26E+04	4.25E-06	3.82E-06	3.61E-06	3.41E-06
Nb	95	3.02E+06	4.34E-06	4.34E-06	4.34E-06	4.34E-06

Nb	97	4.33E+03	3.24E-06	8.82E-07	4.65E-07	2.45E-07
Nb	98	2.86E+00	4.60E-09	0.00E+00	0.00E+00	0.00E+00
Te	116	8.96E+03	3.76E-06	2.00E-06	1.47E-06	1.08E-06
Te	118	5.18E+05	4.34E-06	4.28E-06	4.28E-06	4.25E-06
Te	121	1.45E+06	0.00E+00	1.90E-06	1.90E-06	1.90E-06
I	121	7.63E+03	3.67E-06	1.75E-06	1.22E-06	8.47E-07
Cs	127	2.25E+04	3.01E-06	2.34E-06	2.07E-06	1.83E-06
Ba	127	7.62E+02	1.19E-06	7.46E-10	1.96E-11	5.17E-13
Ba	131	1.02E+06	4.34E-06	8.70E-06	8.70E-06	8.67E-06
La	131	3.54E+03	5.55E-06	1.14E-06	5.17E-07	2.37E-07
La	132	1.73E+04	0.00E+00	3.55E-06	3.03E-06	2.58E-06
La	133	1.41E+04	3.96E-06	2.65E-06	2.18E-06	1.79E-06
La	135	7.02E+04	4.25E-06	3.93E-06	3.79E-06	3.64E-06
Ce	131	6.00E+02	9.51E-07	8.18E-11	8.03E-13	7.92E-15
Ce	132	1.26E+04	1.17E-05	7.51E-06	6.04E-06	4.83E-06
Ce	134	2.73E+05	4.34E-06	4.25E-06	4.19E-06	4.16E-06
Ce	135	6.37E+04	8.50E-06	7.80E-06	7.46E-06	7.14E-06
Ce	137	3.24E+04	2.06E-06	1.01E-05	1.14E-05	1.05E-05
Ce	139	1.19E+07	0.00E+00	1.90E-06	1.90E-06	1.89E-06
Pr	136	7.86E+02	1.22E-06	1.58E-07	4.65E-09	1.37E-10
Pr	137	4.61E+03	9.48E-06	4.94E-06	2.71E-06	1.48E-06
Pr	138	8.70E+01	0.00E+00	5.52E-08	8.03E-22	1.17E-35
Pr	139	1.59E+04	5.95E-06	1.07E-05	9.02E-06	7.57E-06
Nd	136	3.04E+03	2.88E-06	4.54E-07	1.82E-07	7.31E-08
Nd	137	2.31E+03	5.12E-06	4.51E-07	1.35E-07	4.08E-08
Nd	138	1.81E+04	1.56E-05	1.14E-05	9.83E-06	8.44E-06
Nd	139	1.78E+03	8.82E-06	3.76E-07	7.92E-08	1.67E-08
Nd	140	2.91E+05	3.76E-05	3.67E-05	3.64E-05	3.61E-05
Nd	141	8.96E+03	9.48E-06	1.20E-05	8.79E-06	6.45E-06
Pm	138	1.94E+02	3.12E-07	8.24E-20	5.14E-26	3.21E-32
Pm	139	2.49E+02	3.99E-07	6.33E-17	9.28E-22	1.36E-26
Pm	140	9.20E+00	8.79E-08	0.00E+00	0.00E+00	0.00E+00
Pm	141	1.25E+03	8.29E-06	1.58E-07	1.73E-08	1.90E-09
Pm	142	4.05E+01	5.29E-07	8.35E-08	4.42E-08	2.34E-08
Pm	143	2.29E+07	3.58E-05	4.28E-05	4.28E-05	4.28E-05
Pm	145	5.59E+08	4.34E-06	4.34E-06	4.34E-06	4.34E-06
Pm	149	1.91E+05	4.31E-06	4.19E-06	4.13E-06	4.08E-06
Sm	138	1.80E+02	2.89E-07	8.03E-21	1.65E-27	3.38E-34
Sm	140	8.89E+02	1.36E-06	2.45E-09	1.08E-10	4.80E-12
Sm	141	6.12E+02	2.92E-06	3.01E-10	3.24E-12	3.50E-14
Sm	142	4.35E+03	3.24E-05	8.87E-06	4.71E-06	2.48E-06
Sm	143	5.30E+02	6.76E-06	1.67E-10	8.96E-13	4.77E-15
Sm	145	2.94E+07	4.34E-06	4.34E-06	4.34E-06	4.34E-06
Eu	142	2.40E+00	3.84E-09	0.00E+00	0.00E+00	0.00E+00
Eu	143	1.58E+02	7.60E-07	2.74E-22	6.59E-30	1.58E-37
Eu	144	1.02E+01	1.31E-07	0.00E+00	0.00E+00	0.00E+00
Eu	145	5.12E+05	5.72E-05	6.27E-05	6.33E-05	6.39E-05
Eu	146	3.97E+05	1.73E-05	1.71E-05	1.70E-05	1.68E-05

Ho	161*	6.76E+00	1.84E-21	0.00E+00	0.00E+00	0.00E+00
Ho	163	1.44E+11	1.30E-05	7.51E-05	1.10E-04	1.39E-04
Er	152	1.03E+01	1.65E-08	0.00E+00	0.00E+00	0.00E+00
Er	153	3.71E+01	4.16E-07	7.11E-73	0.00E+00	0.00E+00
Er	154	2.21E+02	4.97E-06	4.51E-17	1.62E-22	5.75E-28
Er	155	3.18E+02	6.85E-06	1.45E-13	2.38E-17	3.90E-21
Er	156	1.17E+03	2.70E-05	2.22E-07	2.08E-08	1.95E-09
Er	157	1.12E+03	4.05E-05	2.98E-07	2.50E-08	2.10E-09
Er	158	8.10E+03	1.21E-04	6.33E-05	4.51E-05	3.21E-05
Er	159	2.16E+03	5.72E-05	6.04E-06	1.68E-06	4.65E-07
Er	160	1.03E+05	1.48E-04	1.75E-04	1.71E-04	1.66E-04
Er	161	1.16E+04	6.82E-05	9.97E-05	8.18E-05	6.45E-05
Er	163	4.50E+03	2.06E-05	6.01E-05	5.23E-05	4.10E-05
Er	165	3.73E+04	0.00E+00	8.50E-06	1.32E-05	1.74E-05
Tm	155	3.40E+01	1.09E-07	1.88E-79	0.00E+00	0.00E+00
Tm	156	8.38E+01	2.69E-07	2.05E-36	8.84E-51	3.82E-65
Tm	157	2.10E+02	3.70E-06	8.90E-18	1.65E-23	3.06E-29
Tm	158	2.41E+02	5.40E-06	4.08E-16	4.10E-21	4.16E-26
Tm	159	5.46E+02	1.83E-05	6.21E-10	3.87E-12	2.42E-14
Tm	160	5.64E+02	2.86E-05	2.15E-09	1.58E-11	1.16E-13
Tm	161	1.98E+03	7.80E-05	5.09E-06	1.25E-06	3.09E-07
Tm	162	1.30E+03	8.38E-05	4.57E-06	5.43E-07	6.47E-08
Tm	163	6.52E+03	1.32E-04	7.83E-05	5.12E-05	3.35E-05
Tm	164	1.20E+02	4.54E-06	1.19E-06	6.47E-07	3.53E-07
Tm	165	1.08E+05	1.43E-04	2.18E-04	2.12E-04	2.07E-04
Tm	166	2.77E+04	4.13E-06	1.05E-05	1.37E-05	1.65E-05
Tm	167	7.99E+05	5.72E-05	2.29E-04	2.53E-04	2.62E-04
Tm	171	6.06E+07	4.34E-06	4.34E-06	4.34E-06	4.34E-06
Tm	173	2.97E+04	4.16E-06	3.44E-06	3.12E-06	2.85E-06
Yb	157	3.86E+01	1.24E-07	7.60E-71	0.00E+00	0.00E+00
Yb	158	9.40E+01	6.04E-07	6.65E-33	1.04E-45	1.62E-58
Yb	159	8.40E+01	9.42E-07	8.47E-36	3.93E-50	1.84E-64
Yb	160	2.88E+02	8.32E-06	2.80E-14	1.85E-18	1.23E-22
Yb	161	2.52E+02	7.69E-06	1.60E-15	2.66E-20	4.45E-25
Yb	162	1.13E+03	7.08E-05	4.94E-07	4.28E-08	3.70E-09
Yb	163	6.63E+02	3.73E-05	1.10E-08	1.69E-10	2.58E-12
Yb	164	4.55E+03	1.41E-04	4.39E-05	2.38E-05	1.30E-05
Yb	165	5.94E+02	4.19E-05	4.74E-08	4.45E-10	4.19E-12
Yb	166	2.04E+05	2.88E-04	3.29E-04	3.24E-04	3.18E-04
Yb	167	1.05E+03	4.54E-05	1.40E-05	5.78E-06	2.36E-06
Yb	169	2.77E+06	2.17E-05	3.35E-05	3.96E-05	4.57E-05
Yb	169*	4.60E+01	3.84E-22	3.47E-75	0.00E+00	0.00E+00
Lu	160	3.61E+01	1.16E-07	2.98E-75	0.00E+00	0.00E+00
Lu	161	7.20E+01	4.62E-07	5.98E-41	1.14E-57	2.17E-74
Lu	162	8.22E+01	1.58E-06	3.27E-36	7.43E-51	1.68E-65
Lu	163	2.38E+02	9.94E-06	5.55E-16	4.86E-21	4.25E-26
Lu	164	1.88E+02	9.36E-06	1.05E-18	4.28E-25	1.74E-31
Lu	165	6.42E+02	4.16E-05	7.05E-09	9.39E-11	1.25E-12

Lu	166	1.59E+02	1.76E-05	1.97E-11	5.29E-19	1.42E-26
Lu	167	3.09E+03	1.61E-04	2.75E-05	1.12E-05	4.60E-06
Lu	168	3.30E+02	2.56E-05	7.11E-07	1.20E-07	2.70E-11
Lu	168*	4.02E+02	1.09E-20	9.31E-27	9.42E-30	9.54E-33
Lu	169	1.23E+05	2.65E-04	2.80E-04	2.73E-04	2.67E-04
Lu	169*	1.60E+02	1.23E-19	6.91E-35	2.07E-42	6.18E-50
Lu	170	1.73E+05	5.23E-05	7.46E-05	8.44E-05	9.36E-05
Lu	170*	6.70E-01	3.64E-21	0.00E+00	0.00E+00	0.00E+00
Lu	171	7.12E+05	3.50E-05	6.62E-05	8.18E-05	9.60E-05
Lu	171*	7.90E+01	6.88E-20	8.96E-51	5.17E-66	2.98E-81
Lu	172	5.79E+05	4.34E-06	4.31E-06	4.28E-06	4.25E-06
Lu	173	4.32E+07	2.17E-05	3.03E-05	3.61E-05	4.31E-05
Lu	174	1.05E+08	1.30E-05	1.30E-05	1.30E-05	1.30E-05
Lu	176	1.14E+18	8.70E-06	8.70E-06	8.70E-06	8.70E-06
Lu	177	5.80E+05	4.34E-06	4.31E-06	4.28E-06	4.25E-06
Lu	178	1.70E+03	2.18E-06	8.03E-08	1.58E-08	3.12E-09
Lu	180	3.42E+02	5.49E-07	4.02E-14	1.22E-17	3.67E-21
Hf	164	1.68E+02	1.62E-06	4.86E-21	3.29E-28	2.26E-35
Hf	165	1.02E+02	2.45E-06	2.95E-30	4.62E-42	7.31E-54
Hf	166	4.06E+02	3.12E-05	3.06E-11	3.29E-14	3.58E-17
Hf	167	1.23E+02	8.09E-06	1.18E-25	1.92E-35	3.12E-45
Hf	168	1.56E+03	9.42E-05	2.65E-06	4.45E-07	7.51E-08
Hf	169	1.94E+02	1.53E-05	1.25E-13	8.01E-20	5.14E-26
Hf	170	5.76E+04	2.38E-04	2.38E-04	2.27E-04	2.16E-04
Hf	171	4.39E+04	1.89E-04	2.57E-04	2.41E-04	2.26E-04
Hf	172	5.90E+07	1.67E-04	3.24E-04	3.32E-04	3.35E-04
Hf	173	8.50E+04	7.17E-05	1.85E-04	2.19E-04	2.44E-04
Hf	174	6.30E+22	9.68E-05	2.92E-04	3.35E-04	3.58E-04
Hf	175	6.05E+06	3.58E-05	7.63E-05	9.65E-05	1.16E-04
Hf	177*	1.08E+00	6.27E-13	0.00E+00	0.00E+00	0.00E+00
Hf	177#	3.08E+03	1.98E-12	3.21E-13	1.30E-13	5.29E-14
Hf	178*	4.00E+00	1.90E-11	0.00E+00	0.00E+00	0.00E+00
Hf	178#	9.78E+08	4.60E-11	4.60E-11	4.60E-11	4.60E-11
Hf	179*	1.87E+01	1.76E-10	0.00E+00	0.00E+00	0.00E+00
Hf	179#	2.17E+06	3.76E-11	3.76E-11	3.73E-11	3.73E-11
Hf	180*	1.98E+04	4.22E-08	3.18E-08	2.77E-08	2.40E-08
Hf	181	3.66E+06	2.20E-05	2.20E-05	2.20E-05	2.20E-05
Hf	182	2.84E+14	1.74E-05	1.74E-05	1.74E-05	1.74E-05
Hf	182*	3.69E+03	5.66E-09	1.24E-09	5.84E-10	2.75E-10
Hf	183	3.84E+03	1.18E-07	2.73E-08	1.32E-08	6.45E-09
Hf	184	1.48E+04	1.97E-11	1.35E-11	1.12E-11	9.28E-12
Hf	185	1.00E+01	2.95E-14	0.00E+00	0.00E+00	0.00E+00
Hf	186	1.00E+01	2.20E-24	0.00E+00	0.00E+00	0.00E+00
Ta	166	3.44E+01	1.10E-07	1.30E-78	0.00E+00	0.00E+00
Ta	167	8.40E+01	2.70E-07	2.42E-36	1.13E-50	5.26E-65
Ta	168	1.46E+02	3.27E-06	6.36E-23	3.61E-31	2.05E-39
Ta	169	2.94E+02	1.27E-05	6.39E-14	5.14E-18	4.13E-22
Ta	170	4.06E+02	2.47E-05	2.42E-11	2.62E-14	2.84E-17

Ta	171	1.40E+03	9.97E-05	1.84E-06	2.54E-07	3.53E-08
Ta	172	2.21E+03	1.50E-04	1.38E-05	3.96E-06	1.12E-06
Ta	173	1.13E+04	2.86E-04	1.91E-04	1.49E-04	1.17E-04
Ta	174	4.25E+03	1.76E-04	9.05E-05	4.94E-05	2.58E-05
Ta	175	3.78E+04	2.25E-04	2.87E-04	2.72E-04	2.53E-04
Ta	176	2.91E+04	1.51E-04	2.32E-04	2.44E-04	2.45E-04
Ta	177	2.04E+05	1.07E-04	2.14E-04	2.45E-04	2.65E-04
Ta	178	5.58E+02	1.69E-05	7.17E-10	4.97E-12	3.47E-14
Ta	178*	5.59E+02	1.24E-12	5.32E-17	3.73E-19	2.60E-21
Ta	179	5.75E+07	3.15E-04	5.55E-04	5.72E-04	5.75E-04
Ta	180*	2.94E+04	7.83E-09	6.47E-09	5.90E-09	5.38E-09
Ta	182	9.94E+06	1.53E-04	1.53E-04	1.53E-04	1.53E-04
Ta	182*	2.83E-01	1.71E-11	0.00E+00	0.00E+00	0.00E+00
Ta	182#	9.50E+02	8.93E-09	2.41E-11	1.30E-12	7.05E-14
Ta	183	4.41E+05	1.48E-04	1.46E-04	1.45E-04	1.45E-04
Ta	184	3.13E+04	2.98E-05	2.49E-05	2.28E-05	2.09E-05
Ta	185	2.94E+03	5.40E-05	8.01E-06	3.12E-06	1.21E-06
Ta	186	6.30E+02	8.64E-08	1.16E-11	1.42E-13	1.75E-15
Ta	187	1.00E+01	2.89E-20	0.00E+00	0.00E+00	0.00E+00
W	170	2.40E+02	1.54E-06	1.05E-16	1.01E-21	9.74E-27
W	171	1.44E+02	2.08E-06	2.36E-23	1.03E-31	4.51E-40
W	172	4.80E+02	2.07E-05	1.71E-10	5.32E-13	1.65E-15
W	173	4.78E+02	2.67E-05	2.10E-10	6.36E-13	1.93E-15
W	174	1.76E+03	1.13E-04	4.62E-06	9.60E-07	1.99E-07
W	175	2.10E+03	1.02E-04	7.80E-06	2.08E-06	5.58E-07
W	176	8.30E+03	2.36E-04	1.23E-04	8.84E-05	6.33E-05
W	177	8.10E+03	2.02E-04	1.15E-04	8.15E-05	5.78E-05
W	178	1.87E+06	3.55E-04	3.73E-04	3.73E-04	3.70E-04
W	179	2.25E+03	2.36E-04	2.36E-05	6.88E-06	2.01E-06
W	179*	3.84E+02	5.32E-08	2.35E-14	1.72E-17	1.26E-20
W	181	1.05E+07	7.63E-04	7.69E-04	7.72E-04	7.75E-04
W	183*	5.20E+00	2.67E-06	0.00E+00	0.00E+00	0.00E+00
W	185	6.49E+06	1.12E-03	1.17E-03	1.18E-03	1.18E-03
W	185*	1.00E+02	4.08E-06	1.81E-30	1.75E-42	1.69E-54
W	187	8.60E+04	7.49E-04	6.99E-04	6.79E-04	6.56E-04
W	188	6.00E+06	2.35E-15	2.35E-15	2.35E-15	2.35E-15
Re	171	1.52E+01	2.44E-08	0.00E+00	0.00E+00	0.00E+00
Re	172	1.50E+01	2.41E-08	0.00E+00	0.00E+00	0.00E+00
Re	173	1.19E+02	1.53E-06	4.80E-27	3.67E-37	2.80E-47
Re	174	1.44E+02	1.16E-06	1.31E-23	5.72E-32	2.50E-40
Re	175	3.48E+02	9.48E-06	9.25E-13	3.21E-16	1.12E-19
Re	176	3.18E+02	6.13E-06	1.30E-13	2.13E-17	3.50E-21
Re	177	8.40E+02	2.46E-05	3.06E-08	1.13E-09	4.16E-11
Re	178	7.92E+02	1.72E-05	1.43E-08	4.31E-10	1.30E-11
Re	179	1.17E+03	2.71E-05	2.22E-07	2.08E-08	1.95E-09
Re	180	1.46E+02	3.53E-06	6.82E-23	3.87E-31	2.20E-39
Re	181	7.20E+04	8.53E-05	7.89E-05	7.60E-05	7.31E-05
Re	182	4.57E+04	2.53E-05	2.24E-05	2.11E-05	1.98E-05

Re	183	6.05E+06	3.90E-05	3.90E-05	3.90E-05	3.90E-05
Re	184	3.28E+06	2.61E-05	2.60E-05	2.60E-05	2.60E-05
Re	187	1.58E+18	1.18E-05	5.90E-05	8.12E-05	1.03E-04